

Kepler Planet Occurrence Rates for Mid-Type M Dwarfs as a Function of Spectral Type

KEVIN K. HARDEGREE-ULLMAN,^{1,2,*} MICHAEL C. CUSHING,¹ PHILIP S. MUIRHEAD,³ AND JESSIE L. CHRISTIANSEN²

¹*The University of Toledo, 2801 W. Bancroft St., Mailstop 111, Toledo, OH 43606 USA*

²*Caltech/IPAC-NEExSci, MC 100-22, 1200 E. California Blvd., Pasadena, CA 91125 USA*

³*Department of Astronomy & The Institute for Astrophysical Research, Boston University, 725 Commonwealth Ave., Boston, MA 02215 USA*

ABSTRACT

Previous studies of planet occurrence rates largely relied on photometric stellar characterizations. In this paper, we present planet occurrence rates for mid-type M dwarfs using spectroscopy, parallaxes, and photometry to determine stellar characteristics. Our spectroscopic observations have allowed us to constrain spectral type, temperatures, and in some cases metallicities for 337 out of 561 probable mid-type M dwarfs in the primary *Kepler* field. We use a random forest classifier to assign a spectral type to the remaining 224 stars. Combining our data with *Gaia* parallaxes, we compute precise ($\sim 3\%$) stellar radii and masses, which we use to update planet parameters and planet occurrence rates for *Kepler* mid-type M dwarfs. Within the *Kepler* field, there are seven M3 V to M5 V stars which host 13 confirmed planets between 0.5 and 2.5 Earth radii and at orbital periods between 0.5 and 10 days. For this population, we compute a planet occurrence rate of $1.19^{+0.70}_{-0.49}$ planets per star. For M3 V, M4 V, and M5 V, we compute planet occurrence rates of $0.86^{+1.32}_{-0.68}$, $1.36^{+2.30}_{-1.02}$, and $3.07^{+5.49}_{-2.49}$ planets per star, respectively.

Keywords: stars: planetary systems — stars: fundamental parameters — stars: late-type — stars: low-mass

1. INTRODUCTION

The NASA *Kepler* mission (Borucki et al. 2010) revolutionized astrophysics and planetary science. *Kepler* has enabled the discovery of 2,342 new exoplanets and an additional 2,421 planet candidates.¹ Four years of data from the original *Kepler* mission have provided light curves for nearly 200,000 stars (Mathur et al. 2017) from which we can estimate the statistical distribution of planet properties within our Galaxy.

Kepler was designed to detect Earth-sized planets in the habitable zones of Sun-like (F, G, and

K) stars. M dwarfs ($2,300\text{ K} \lesssim T_{\text{eff}} \lesssim 3,900\text{ K}$, $0.1 R_{\odot} \lesssim R_{\star} \lesssim 0.6 R_{\odot}$, $0.07 M_{\odot} \lesssim M_{\star} \lesssim 0.6 M_{\odot}$) comprise about 70% of the nearby stellar population, by number (Henry et al. 2006; Bochanski et al. 2010), though they only constitute about 2.5% of the targets *Kepler* observed (Dressing & Charbonneau 2015, hereafter DC15). The smaller size of these stars makes it easier to detect the presence of smaller transiting planets. For example, the transit depth for an Earth-radius planet transiting a solar metallicity M0 V star would be 3 times deeper than the same planet transiting a G2 V Sun-like star, and nearly 70 times deeper for an M7 V star. Fortuitously, the low luminosity of M dwarfs means the habitable zone is closer to the star, thus increasing the chance of detecting a transiting planet in the habitable zone over a finite observing period (Nutzman & Charbonneau 2008). For example, an Earth-sized planet in the habitable zone of an M4 V star orbits once every two weeks as opposed to once a year for a Sun-like G star.

Planet occurrence rates increase toward later spectral types within the *Kepler* field. Using the first three quarters of *Kepler* data, Howard et al. (2012) measured the

Corresponding author: Kevin K. Hardegree-Ullman
kevinkhu@caltech.edu

* Visiting astronomer, Kitt Peak National Observatory, National Optical Astronomy Observatory, which is operated by the Association of Universities for Research in Astronomy (AURA) under a cooperative agreement with the National Science Foundation. Visiting Astronomer at the Infrared Telescope Facility, which is operated by the University of Hawaii under contract NNH14CK55B with the National Aeronautics and Space Administration.

¹ http://exoplanetarchive.ipac.caltech.edu/docs/counts_detail.html, as of April 2019

planet occurrence rate for M0 to F2 dwarfs for planets with radii between 2 and $4 R_{\oplus}$ and found that these small planets are seven times more abundant around cool stars (3,600 to 4,100 K) than hot stars (6,600 to 7,100 K). More recent work by [Mulders et al. \(2015a\)](#) found the occurrence rate of planets with radii between 1 and $4 R_{\oplus}$ around M dwarfs to be two times higher than for G stars, and three times higher than for F stars. [Dressing & Charbonneau \(2013, hereafter DC13\)](#) focused specifically on stars with temperatures below 4,000 K in Q1 to Q6 of *Kepler* data and found the occurrence rate of 0.5 to $4 R_{\oplus}$ planets with orbital periods shorter than 50 days to be $0.90_{-0.03}^{+0.04}$ planets per star. Separating these stars into warmer ($T_{\text{eff}} > 3,400$ K) and cooler ($T_{\text{eff}} < 3,400$ K) groups, they find the occurrence rate of Earth-sized planets (0.5 to $1.4 R_{\oplus}$) to be consistent at around 0.5 planets per star, but the rate of larger planets (1.4 to $4.0 R_{\oplus}$) is three times higher for the warmer stars, $0.61_{-0.06}^{+0.08}$ compared to $0.19_{-0.05}^{+0.07}$. Using the full *Kepler* data set, [DC15](#) updated their M dwarf planet occurrence data rate for 1 to $4 R_{\oplus}$ planets with orbital periods shorter than 200 days to be 2.5 ± 0.2 planets per star, but they do not make a distinction between early and mid-type M dwarfs. [Gaidos et al. \(2016b\)](#) computed an overall *Kepler* M dwarf planet occurrence rate of 2.2 ± 0.3 for orbital periods shorter than 180 days, consistent with [DC15](#). Focusing specifically on mid-type M dwarfs, [Muirhead et al. \(2015\)](#) calculated a compact multiple occurrence rate of $21_{-5}^{+7}\%$, assuming a radius of $0.2 R_{\odot}$ for all mid-type M dwarfs.

Computing planet occurrence rates requires measurements of stellar radii (R_{\star}) for all stars in the sample population. In the absence of direct measurements, R_{\star} for the M dwarfs in the *Kepler* Input Catalog (KIC) was derived from optical and infrared photometry ([Batalha et al. 2010](#); [Brown et al. 2011](#)). [Brown et al. \(2011\)](#) noted that stellar parameters in the KIC are unreliable at $T_{\text{eff}} < 3,750$ K because the models they use are calibrated to work best for Sun-like stars. [DC13](#), [Gaidos \(2013\)](#), and [Huber et al. \(2014\)](#) addressed this issue by using stellar models more suited to later type stars (e.g., Dartmouth Stellar Evolution Database; [Dotter et al. 2008](#)) to reclassify the set of cooler stars in the KIC. These updated measurements of R_{\star} , based on photometry, still have a wide range of uncertainties with an average around 30% ([Mathur et al. 2017](#)). An uncertainty this large can mean the difference between several spectral sub-types, and for a transiting planet this propagates to a 30 to 40% planet radius uncertainty.

Combining long-baseline optical interferometry with trigonometric parallax measurements yields direct measurements of stellar radii with uncertainties between 1%

and 5%; however, this method is currently limited to bright ($V \lesssim 11$), nearby stars (e.g., [Ségransan et al. 2003](#); [Boyajian et al. 2012](#); [von Braun et al. 2014](#)). These precise radius measurements can, however, be used to calibrate empirical relationships between radius and other measurable parameters (e.g., [Boyajian et al. 2012](#); [Mann et al. 2015](#)). For example, [Mann et al. \(2015, hereafter M15\)](#) derive M_{K_s} vs. R_{\star} and T_{eff} vs. R_{\star} relationships for K7 through M7 dwarfs, which constrain stellar radii to $\sim 3\%$ and $\sim 15\%$, respectively. [Gaidos et al. \(2016b\)](#) used these relationships to update the stellar properties of over 4,000 *Kepler* M dwarfs based on temperatures, metallicities, and distances derived from photometry and proper motions. These measurements constrain stellar radii to $\sim 15\%$.

With moderate resolution spectra, we can precisely determine spectral type and measure stellar properties such as temperature and metallicity. Having accurate spectral types for a specific population (e.g., mid-type M dwarfs) allows us to assess trends in planet occurrence rates for that population as a function of spectral type, like the assessment of F, G, K, and early M dwarf planet occurrence rates by [Howard et al. \(2012\)](#). In large stellar catalogs, such as the KIC, it is difficult to obtain a spectrum of each star, so photometric selection criteria are typically used to identify specific stellar populations (e.g., [Brown et al. 2011](#); [Dressing & Charbonneau 2013](#); [Gaidos 2013](#); [Huber et al. 2014](#); [Gaidos et al. 2016b](#)). Efforts to spectroscopically classify nearly 5,000 photometrically-identified late-type K and M dwarfs in the *Kepler* field by [Mann et al. \(2012\)](#), [Muirhead et al. \(2012\)](#), [Mann et al. \(2013b\)](#), and [Martín et al. \(2013\)](#) have yielded spectra for only 2% of the sample ([DC15](#)). While selection criteria aim to minimize stellar outliers, they are not impervious to contamination. Spectra allow us to identify any interlopers (such as giant stars) that selection criteria might not cull.

In this paper we present spectroscopic observations of 333 M dwarfs and 4 M giants in the *Kepler* field, from which we derive spectral types, effective temperatures, and metallicities. Thanks to the European Space Agency’s *Gaia* mission ([Gaia Collaboration et al. 2016](#)), nearly all the stars in the *Kepler* field now have trigonometric parallax measurements ([Berger et al. 2018](#)). Over 90% of our targets have *Gaia* parallax measurements, which we use to compute M_{K_s} . We apply the empirical relationships of [M15](#) and [Mann et al. \(2019\)](#) to measure radii and masses for our stars. With these updated stellar properties, we refine the properties for the 13 confirmed planets around mid-type M dwarfs. We then compute the total planet occurrence rate for mid-type M dwarfs, individual occurrence rates for M3 V,

M4 V, and M5 V stars, and compact multiple occurrence rates.

In Section 2 we describe our target selection, spectroscopic observations, and *Gaia* data. We explain our methods for determining stellar properties in Section 3, and refine our sample to reject giant stars and close binaries in Section 4. In Section 5 we identify the planets around mid-type M dwarfs in the *Kepler* field, which we use for our planet occurrence rate calculations in Section 6. We conclude with a discussion in Section 7.

2. TARGET SELECTION, OBSERVATIONS, AND DATA REDUCTION

Using revised KIC temperature estimates, DC13 identified 202 stars with $T_{\text{eff}} \lesssim 3,300$ K. Muirhead et al. (2015) identified 509 probable mid-type M dwarfs from KIC photometry using the following color selection criteria: $r - J > 3.2$ to identify red objects, and $J - K < 0.0555 \times (r - J) + 0.7622$ to remove giant stars. The union between these samples produces 561 probable mid-type M dwarfs which we targeted in this study. In total, we observed 337 of the 561 targets (60%), obtaining optical spectra of 327 stars and near-infrared spectra of 82 stars. We have both optical and infrared spectra for 72 targets. Magnitude distributions of our targets in r -band and K_s -band are shown in Figure 1, including the distributions of targets we observed.

2.1. WIYN

In observing semester 2015B, NASA and NSF implemented Stage 1 of the Exoplanet Observational Research (NN-EXPLORE) program, enabling community access to about 100 nights per year on the 3.5-meter WIYN² telescope on Kitt Peak at least through commissioning of the extreme precision Doppler spectrometer NEID (Schwab et al. 2016). We have made use of the fiber-fed multi-object spectrograph Hydra (Barden et al. 1994) on WIYN for this project. The *Kepler* field spans a 12 degree diameter, making the one degree diameter field-of-view of Hydra advantageous. We collected spectra over five observing semesters beginning in September 2015 (NOAO Program IDs 2015B-0280, 2016A-0328, 2016B-0111, 2017A-0185, 2017B-0095; PI: K. Hardegree-Ullman). In total, we observed 287 targets with WIYN.

² The WIYN Observatory is a joint facility of the University of Wisconsin-Madison, Indiana University, the National Optical Astronomy Observatory and the University of Missouri.

Each Hydra field configuration contained an average of five mid-type M dwarf targets with $V < 18.5$ ³. We used the bench spectrograph camera and the red optimized fiber cable containing 90 fibers. The 316 lines mm^{-1} grating and the G5 filter were used to obtain spectra spanning 5,000 to 10,000 Å with an average resolving power $R = \lambda/\Delta\lambda \approx 1,420$. Most fields were observed in three consecutive 1,200 second exposures to mitigate the effect of cosmic rays and to yield a signal-to-noise (S/N) of at least 30 per resolution element for targets with $V < 18.5$. At the beginning and end of each night we obtained bias, dome flat field, and copper-argon wavelength calibration frames. After each field observation, we obtained a spectrum of a nearby bright G0 star at a similar airmass to be used for telluric correction. At least once each night we observed a spectrophotometric standard star for relative flux calibration.

The data were reduced using IRAF⁴ and custom IDL routines. Each image was first corrected for readout bias using the overscan strip, then trimmed to remove this region. An average bias was then created and subtracted from the rest of the images. The *dohydra* IRAF routine was used for aperture extraction, flat fielding, dispersion correction, and sky subtraction. Sky spectra were created from 5 to 10 sky fibers placed in random positions distributed throughout each field. Sky subtraction removed OH atmospheric emission, which is problematic at wavelengths redder than 6,000 Å. Individual exposures were then combined, and a relative flux calibration was performed on all targets using a spectrophotometric standard star. We developed a custom IDL script to interpolate across a G0 star spectrum where there is known atmospheric absorption, and divide these regions out of our M dwarf spectra to remove terrestrial atmospheric absorption features. We shift each spectrum in wavelength to the source star's rest frame by cross-correlation with the closest matching M dwarf template from Bochanski et al. (2007). We find the closest matching M dwarf template from a by-eye comparison of each spectrum to each template, normalized to 8,350 Å.

2.2. Discovery Channel Telescope

³ KIC photometry was converted to V -band magnitudes using the transformation $V = g - 0.5784 \times (g - r) - 0.0038$, <http://www.sdss3.org/dr8/algorithms/sdssUBVRITransform.php#Lupton2005>

⁴ IRAF is distributed by the National Optical Astronomy Observatories, which are operated by the Association of Universities for Research in Astronomy, Inc., under cooperative agreement with the National Science Foundation.

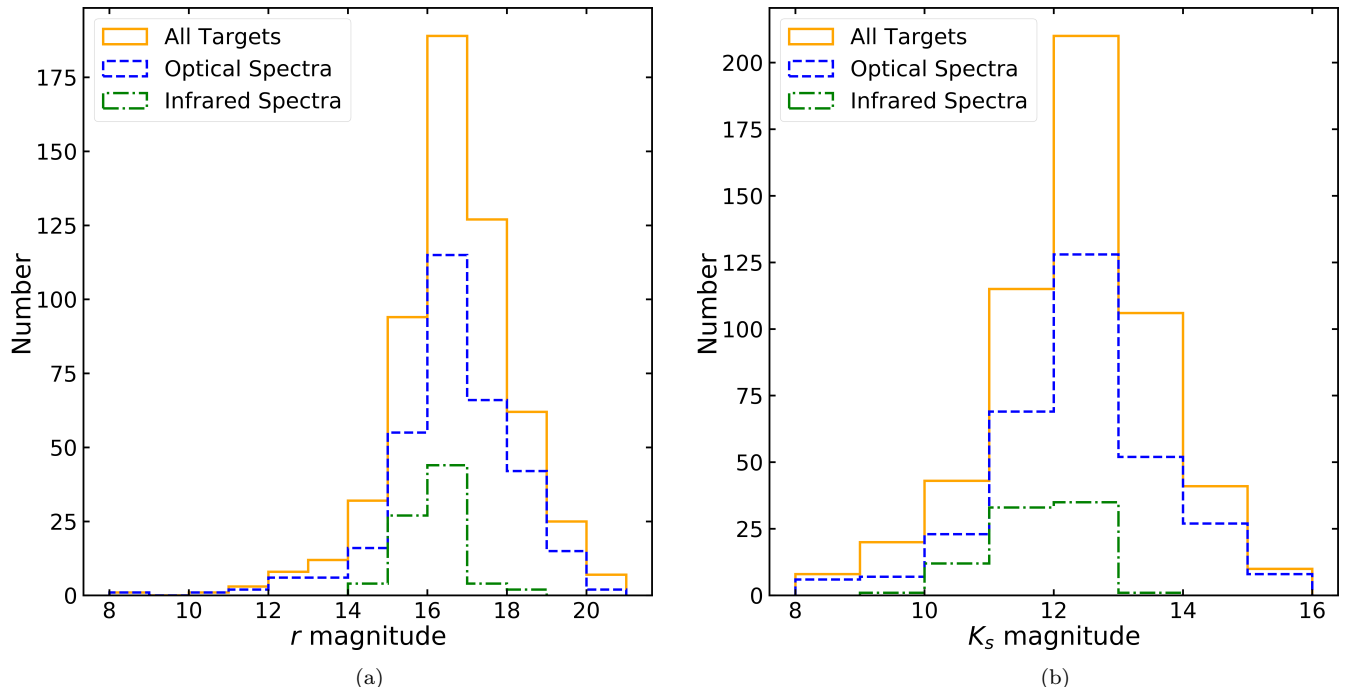


Figure 1. Magnitude distributions in (a) r -band and (b) K_s -band of *Kepler* targets for this survey. The orange solid line histograms represent all targets, the blue dashed line histograms are the targets for which we have an optical spectrum, and the red dashed dotted line histograms show targets for which we have an infrared spectrum. The optical spectra distribution closely follows the distribution of all targets in the sample. Targets were selected to optimize observation efficiency with WIYN by maximizing the number of targets observed per field configuration. Several fainter targets were also observed with the Discovery Channel Telescope. This strategy allowed us to effectively observe a random sample representing the total target set. Almost all stars with infrared spectra have $K_s < 13$, since fainter targets necessitate much longer integration times to obtain sufficient S/N to measure stellar properties.

About 90 of our targets have V -band magnitudes fainter than 18.5, which would require integration times longer than one hour using WIYN to achieve a S/N of 30. We therefore used the DeVeney spectrograph on the 4.3-meter Discovery Channel Telescope (DCT) to observe some of these fainter targets over four observing runs, collecting spectra of 49 stars. We observed 17 of these stars with WIYN because they were within one of the observed WIYN fields. These targets are used to check for consistency between the two telescopes, though the DCT data are higher resolution.

The DeVeney spectrograph is a single-slit instrument with a deep depletion e2v CCD. The 400 grooves mm^{-1} grating and OG570 filter were used to obtain spectra spanning 6,300 to 9,700 \AA with $R \approx 2,850$. Total integration times varied in order to achieve a S/N similar to WIYN targets, and at least three consecutive exposures were taken of each target to mitigate cosmic rays in the data reduction. Calibrations were the same as for WIYN, except for the neon-argon lamps used for wavelength calibration. Data reduction was again performed in IRAF using the same steps as for WIYN data, but with single slit routines instead of *dohydra*.

2.3. IRTF

We used the SpeX spectrograph (Rayner et al. 2003) on the NASA Infrared Telescope Facility (IRTF) on Maunakea to observe 82 targets over 12 partial nights (Program IDs 2016A-981, 2017A-106, 2017B-021; PI: K. Hardegree-Ullman). We used SpeX in SXD mode with a $0''.3 \times 15''$ slit to obtain 0.8 to 2.4 μm spectra at $R \approx 2,000$. We observed using the ABBA nod pattern with at least three exposures for each target. Exposure times were shorter than 120 seconds to minimize effects from atmospheric OH line variability. For most targets we achieved a S/N of at least 50 per resolution element. An A0 V star was observed within 0.1 airmasses of each target to be used for telluric correction and flux calibration. Flat field and thorium-argon lamp calibrations were taken after each A0 V star observation.

Spectra were reduced using *Spextool* (v. 4.2; Cushing et al. 2004), which performs flat fielding, wavelength calibration, sky subtraction, and spectrum extraction. We used the *xtellcor* IDL package (Vacca et al. 2003) for telluric correction. As with each optical spectrum, we shift each infrared spectrum in wavelength to the source

star’s rest frame by cross-correlating with a spectrum of corresponding spectral type from the IRTF spectral library (Cushing et al. 2005; Rayner et al. 2009).

2.4. LAMOST

The Large Sky Area Multi-Object Fiber Spectroscopic Telescope (LAMOST; Cui et al. 2012) is a 4-meter class telescope designed to survey stars and galaxies in the northern hemisphere. Its 4,000 fiber multi-object spectrograph has a wavelength range of 3,690 to 9,100 Å at $R \approx 1,800$. As of data release 4, over 7.6 million⁵ spectra have been gathered in total. There are LAMOST spectra for 17 of our *Kepler* targets, including 8 targets we did not observe with WIYN or the DCT. This brings our total optical spectra count to 327 targets.

2.5. Gaia

The *Gaia* mission has provided parallax measurements for over 1.3 billion sources in second data release (Gaia Collaboration et al. 2018). Bailer-Jones (2015) and Bailer-Jones et al. (2018) note that simply inverting the parallax does not always produce reliable distances. Instead, distances must be inferred via probabilistic analysis, which Bailer-Jones et al. (2018) performed on all targets in the second *Gaia* data release, providing distance measurements and uncertainties. We use the *Gaia/Kepler* cross-match database⁶ to obtain the Bailer-Jones et al. (2018) *Gaia* distances to our *Kepler* stars. In total, 532 of our targets cross-match with a *Gaia* target within 4'', the *Kepler* pixel size. We also check the difference between the *Gaia* *G*-band ($\gtrsim 20\%$ transmission between 4,000 and 9,000 Å; Evans et al. 2018) and *Kepler* *Kp*-band ($\gtrsim 20\%$ transmission between 4,300 and 8,900 Å⁷) magnitudes. For any target with an absolute *G* – *Kp* magnitude difference greater than 2, we discard the parallax measurement in our analysis, which applies to KIC 02164791, KIC 03330684, KIC 07729309, and KIC 10665619.

3. STELLAR PROPERTIES

We seek to determine planet occurrence rates for mid-type M dwarfs using revised stellar radius measurements derived from spectra, photometry, and parallaxes. About 95% of our targets have parallax measurements, which allows us to compute absolute magnitudes in the *r*, *J*, and *K_s*-bands for use in computing stellar properties (Section 3.1). For the 337 targets with spectra, we

do a by-eye comparison to spectral templates to determine spectral types. There are 224 targets for which we do not have spectra, so we use a machine learning technique to identify spectral type from photometry (Section 3.2). Using a spectral type vs. temperature relationship, we derive stellar temperatures (Section 3.3). For targets with infrared spectra, we determine metallicity (Section 3.4). We apply the M_{K_s} vs. radius and M_{K_s} vs. mass relationships of M15 and Mann et al. (2019) to derive stellar radii and masses for targets with parallax measurements. For the remaining targets, we derive radii from a temperature vs. radius relationship (Section 3.5) and masses from a radius vs. mass relationship (Section 3.6). With our updated spectral types, we isolate mid-type M dwarfs, and compute planet occurrence rates for spectral types M3 V to M5 V using our new stellar properties (Section 6). We present all derived stellar parameters in Tables 3 and 4.

3.1. Absolute Magnitudes

For targets with *Gaia* parallax measurements, we compute absolute magnitudes M for Sloan Digital Sky Survey (SDSS; York et al. 2000) *r*-band and Two Micron All-Sky Survey (2MASS; Skrutskie et al. 2006) *J* and *K_S*-bands using

$$M = m - 5[\log_{10}(d) - 1] - A, \quad (1)$$

where m is the apparent magnitude for a photometric band, d is the distance in parsecs, and A is the extinction for that photometric band. We compute reddening vectors using the 3D dust maps of Green et al. (2018) with the Python package `dustmaps`. We find extinction for each band by multiplying the reddening vectors by the extinction coefficients R from Green et al. (2018), which are 2.483, 0.650, and 0.161 for *r*, *J*, and *K_s* bands, respectively. We calculate absolute magnitudes and their associated uncertainties for each band using the following Monte Carlo (MC) analysis. For each measured parameter we generate 10^4 random samples from a Gaussian distribution and combine these distributions for each calculation. The uncertainties for each quantity are symmetric or nearly symmetric within a few percent, so we use the mean of any asymmetric uncertainty to draw our Gaussian distribution. The absolute magnitude is then the median value of the posterior distribution, and we adopt the 16th and 84th percentiles as the uncertainties.

3.2. Spectral Type

We determine optical spectral types by comparing our spectra to the SDSS M dwarf spectral templates of Bochanski et al. (2007), following the methods of

⁵ <http://dr4.lamost.org/>

⁶ <http://gaia-kepler.fun/>

⁷ <https://keplergo.arc.nasa.gov/CalibrationResponse.shtml>

Kirkpatrick et al. (1991). The template spectra span a wavelength range of 3,800 to 9,200 Å with $R \approx 1,800$. Target spectra are normalized to the same wavelength as the template spectra (8,350 Å) and we do a by-eye comparison to find the closest matching spectrum to the nearest half spectral type. Ten of our targets were only observed with IRTF. For these targets, we determine spectral type in the same manner as our optical spectra, except we use M dwarfs in the IRTF Spectral Library for comparison (Cushing et al. 2005; Rayner et al. 2009).

It is always best to determine spectral type from a spectrum rather than photometry, however, this is not always economical with a large target sample and limited resources. For the 224 stars in our sample that lack a spectrum, we use the `RandomForestClassifier` routine from the `scikit-learn` (Pedregosa et al. 2011) Python package to classify these targets with r , J , and K_s -band photometry. For our training sample, we use the extinction corrected photometry and spectral types from West et al. (2011), who visually inspected over 70,000 M dwarf spectra from SDSS. We truncate this data set to include spectral types M0 to M8, and use the color cut $J - K_s < 0.0555 \times (r - J) + 0.7622$ to reflect the targets in our sample. From these 48,978 targets, we randomly select 1,500 from each spectral type to minimize sample bias, reducing our input sample to 13,500 targets. Using the $r - J$ and $J - K_s$ colors along with spectral type, we train the random forest classifier on a random subset of 75% of the total input sample. The remaining 25% of the input sample is used to determine how well the classifier performs. Figure 2 compares the observed spectral type from spectra to the predicted spectral type from the classifier. Over 90% of the predicted classifications are within one spectral type of the observed spectral type, so we adopt an uncertainty of ± 1 spectral type for our photometric classifications.

We run the trained classifier on the photometry for both our spectroscopically observed and unobserved targets. In the case of the 530 targets for which we have *Gaia* parallax measurements, we use extinction corrected absolute magnitudes to compute $r - J$ and $J - K_s$ colors. The average difference between the colors computed from absolute magnitudes versus apparent magnitudes is about 0.03 for each color, which is the small effect of the reddening correction. For the remaining 31 targets without parallax measurements, we use apparent magnitudes to compute colors. The classifier predicts 86% of the spectral types of our spectroscopically observed sample to within one spectral type, however, it over-predicts M3 V by a factor of 2, and significantly under-predicts M2 V and M7 V, as shown in Figure 3 a. For the photometric sample, the distribution of spec-

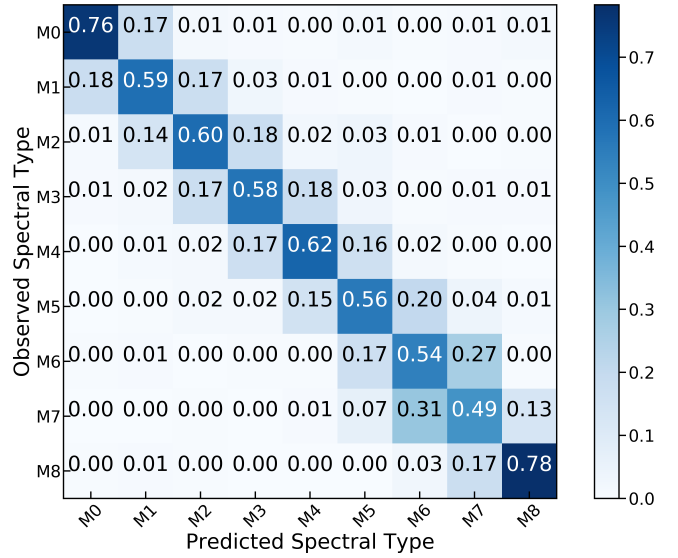


Figure 2. Comparison of the fraction of predicted classifications in each spectral type bin versus observed spectral type from a random forest classification using photometry from the West et al. (2011) M dwarf sample. Over 90% of the predicted classifications are within one spectral type of the observed spectral type.

tral types roughly follows the same distribution as the spectroscopic sample. We also show the spectral type distribution for the entire sample in Figure 3 b. Since we effectively observed a random subset of mid-type M dwarfs in the *Kepler* field, we expect the photometrically classified targets to follow a similar spectral type distribution to the spectroscopically classified targets, and thus we are confident in the results from the photometric classification.

3.3. Effective Temperature

Direct measurement of effective temperatures requires both bolometric flux and interferometric angular diameter measurements. Due to the distance and faintness of these stars, interferometric observations are not currently possible. Using the spectral types and effective temperatures of the 183 stars in Table 5 of M15, we determine a linear spectral type vs. effective temperature relationship:

$$T_{\text{eff}} = -168.37 \times SpT + 3914.65, \quad (2)$$

where SpT is the spectral type between -1 for K7 V and 7 for M7 V. We adopt this as a uniform temperature scale across our spectroscopic and photometric sample. The residual $1-\sigma$ scatter of our fit to the M15 spectral types and temperatures is 64 K, which we add in quadrature to the typical 60 K spectroscopic measurement uncertainties. This yields 88 K, which we adopt as our temperature uncertainty.

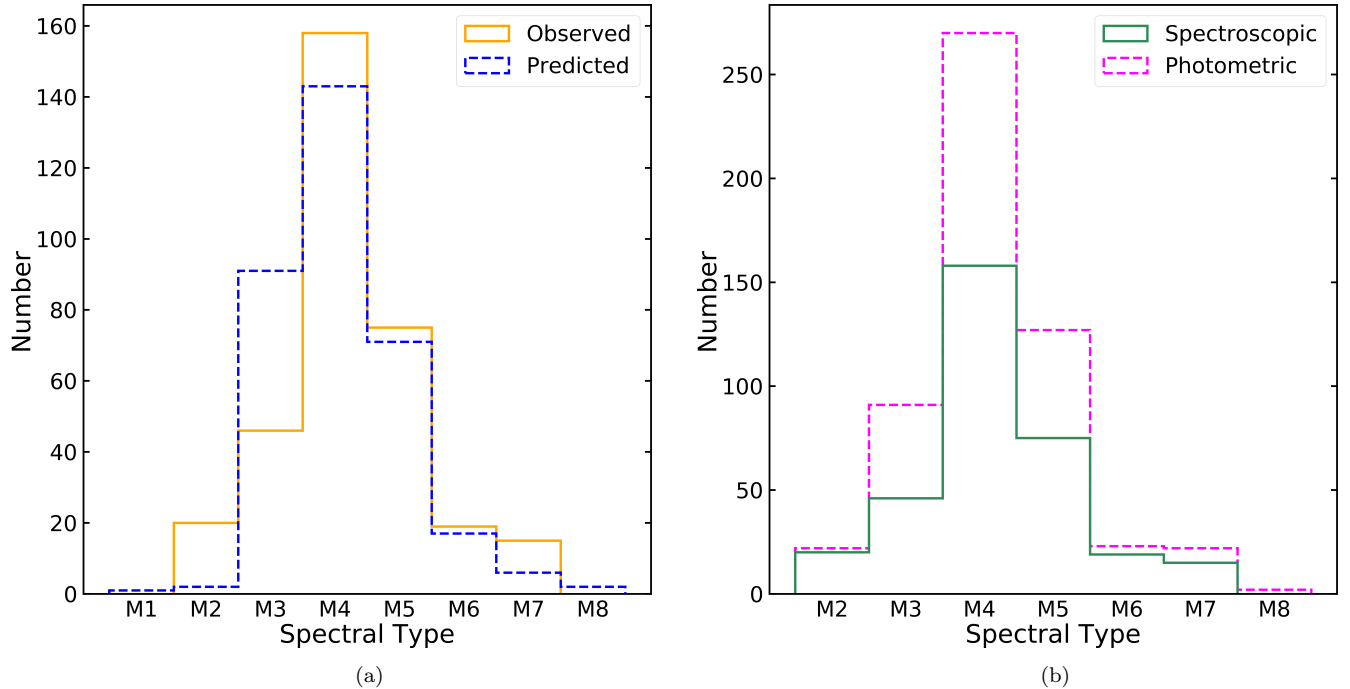


Figure 3. (a) Comparison of observed (solid orange) versus predicted (dashed blue) spectral type distributions using the random forest classifier on the *Kepler* targets we have spectroscopically classified. (b) The spectral type distribution for our entire *Kepler* sample using results from spectra for observed targets (solid green), and the classifier (dashed magenta) on stars without spectra. The photometric histogram is stacked on top of the spectroscopic histogram. For these histograms, stars with half spectral types are rounded up to the nearest integer type.

Pecauc & Mamajek (2013) determine effective temperatures for each sub-type of main sequence stars by taking the median values of published effective temperatures in the literature. As a consistency check to our M15 fit, we take the most recent list of all reported values used to compute the median effective temperature for each sub-type⁸ between K7 V and M9 V (280 stars) and fit a linear relationship. This results in $T_{\text{eff}} = -166.96 \times SpT + 3868.39$, with a 107 K 1- σ scatter. This relationship gives temperatures on average 40 K cooler than our temperatures. We also compare our temperatures to the M dwarf temperature scale of Rajpurohit et al. (2013), which are on average 76 K cooler than our temperatures. All three methods yield temperatures which are consistent within the measurement uncertainties.

3.4. Metallicity

We computed metallicities (specifically, iron abundance, [Fe/H]) for 82 targets we observed with SpeX on IRTF. Mann et al. (2013a, 2014) determined metallicity of M dwarfs in wide binary systems with an F, G, or K primary star, and computed empirical relationships be-

tween metallicity and equivalent widths of Na I and Ca I using infrared spectra from SpeX. Our metallicity measurements using these relationships are listed in Table 3. We did not obtain infrared spectra of any of the mid-type M dwarf planet hosts (Table 2), however, we adopt the metallicity measurements of Kepler-42, Kepler-445, and Kepler-1650 from Mann et al. (2017), Kepler-446 and Kepler-1582 from Muirhead et al. (2014), and Kepler-1649 from Angelo et al. (2017). All of these metallicity measurements were made using the same relationships from Mann et al. (2013a). The only planet host for which we do not have a metallicity measurement is Kepler-1646.

3.5. Radius

For the 95% of targets with distance measurements, we apply the M_{K_s} vs. R_* and M_{K_s} vs. [Fe/H] vs. R_* relationships of M15 to compute stellar radii, which have model fit uncertainties of 2.89% and 2.70%, respectively. We employ the same MC analysis from Section 3.1 to assess parameter uncertainties, and add them to the model uncertainties in quadrature, which yields a median 3.13% and 2.85% radius uncertainty, respectively.

Not all of our targets have distance measurements, so we rely on the M15 T_{eff} vs. R_* and T_{eff} vs. [Fe/H] vs. R_* relationships to get the remaining stellar radii. Adding

⁸ <http://www.pas.rochester.edu/~emamajek/spt/>

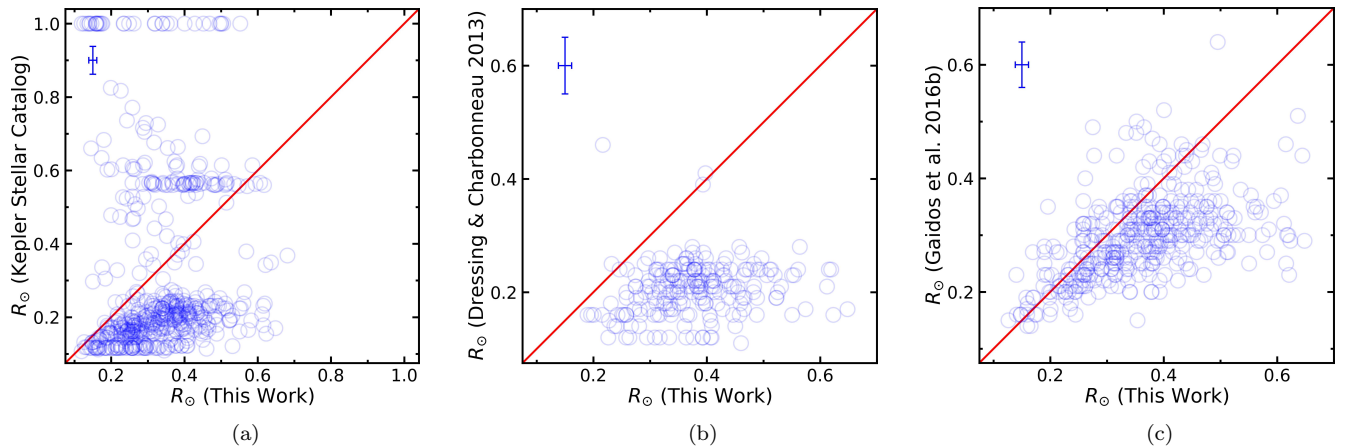


Figure 4. (a) Comparison of our radius measurements of *Kepler* M dwarfs to radii from the *Kepler* Stellar Catalog (Mathur et al. 2017). We do not include 17 targets from the *Kepler* Stellar Catalog with $R_{\star} > 1 R_{\odot}$. The 1:1 reference line is plotted in red, and median uncertainties are shown in the upper left corner. The histograms show the radius measurement distributions. (b) Comparison of our radius measurements to those from DC13 for the 213 targets found in both samples. (c) Comparison of our radius measurements to those from Gaidos et al. (2016b) for the 399 targets found in both samples. Our radii are generally larger than previous measurements.

in quadrature the 13.4% (T_{eff} vs. R_{\star}) and 9.3% (T_{eff} vs. $[\text{Fe}/\text{H}]$ vs. R_{\star}) uncertainties to values from the MC analysis, we yield median uncertainties of 20.6% and 18.6%, respectively, for these targets.

In Figure 4 we compare our new stellar radius measurements to those reported in the *Kepler* Stellar Catalog (Mathur et al. 2017), 213 of our targets also found in DC13, and 399 stars in Gaidos et al. (2016b). Both the *Kepler* Stellar Catalog and DC13 show a similar radius distribution for most targets, with a peak near $0.2 R_{\odot}$, whereas our measurements are generally larger by $\sim 58\%$. Our radii are more consistent with those reported in Gaidos et al. (2016b), but our use of distances from *Gaia* yield more precise values of M_{K_s} , resulting in $\sim 20\%$ larger radii.

3.6. Mass

We apply the M_{K_s} vs. M_{\star} relationship of Mann et al. (2019) to compute stellar masses of targets with distance measurements using the Python code provided with that paper⁹. This yields median uncertainties of 2.59% and 2.64% for targets with and without metallicity measurements, respectively. For the 28 targets without M_{K_s} measurements we need another method to compute mass. We fit the mass and radius measurements for 183 M dwarfs in M15 with a third degree polynomial using the `polyfit` routine in the `numpy` (Oliphant 2015) Python package and find:

$$M_{\star} = -0.01 + 0.63R_{\star} + 1.34R_{\star}^2 - 0.99R_{\star}^3. \quad (3)$$

⁹ https://github.com/awmann/M_-MLK-

The root-mean square scatter of this fit is 3.75%. We apply Equation 3 to the targets for which we do not have distance measurements in the same manner as our previous model fits and yield a median 33.2% mass uncertainty for these targets.

4. REFINING THE SAMPLE

Our target selection criteria were chosen to isolate M dwarfs, but that does not preclude a few giant or binary interlopers. From our spectra, we identify four giants (Section 4.1), two eclipsing binaries, four potential white dwarf-M dwarf binaries (Section 4.2), and 15 probable binaries from the *Gaia* data (Section 4.3).

4.1. Giants

Spectroscopic indicators of M giants include weak Na D, K I, and Na I absorption, significant Ca II absorption, and differing shapes in the CaH2 index compared to M dwarfs (Reid et al. 1995; Mann et al. 2012). The four giants we identify from spectra are KIC 08628971, KIC 10548114, KIC 11495654, and KIC 11913210 (Figure 5). KIC 11913210 is CH Cygni, an S-type symbiotic star system¹⁰ consisting of at least two giant stars (Skopal 2005). We discard these sources in our occurrence rate analysis, reducing our sample to 557 stars.

4.2. Binaries

¹⁰ An S-type star is a cool giant containing zirconium monoxide bands in their spectra (Merrill 1922, 1923). This is not to be confused with an S-type orbit, where a planet orbits a single star in a binary star system.

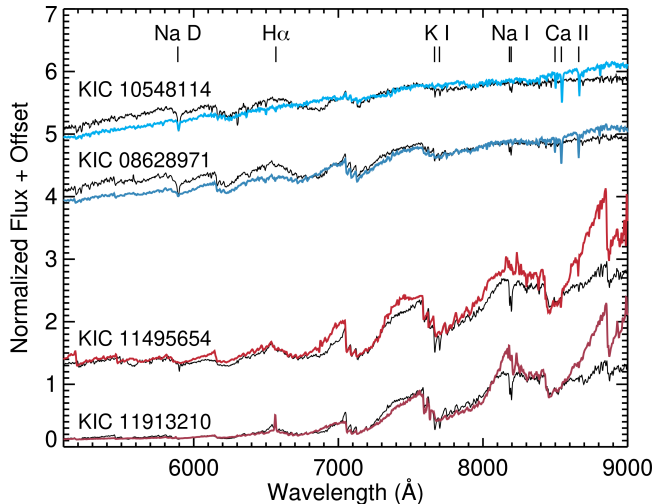


Figure 5. Four giant stars identified in our data (in color), corresponding to two early and two late-type M giants. We plot an M dwarf of similar spectral class (black) to show differences in spectral features. Prominent spectral lines used to delineate dwarf and giant spectra are identified at the top of the plot.

Within the *Kepler* data, 2,909 eclipsing binaries have been identified¹¹, which is $\sim 1.5\%$ of the nearly 200,000 *Kepler* stars observed (Kirk et al. 2016; Abdul-Masih et al. 2016). Two of our targets are eclipsing binaries, KIC 07174349 and KIC 10002261, which we spectral type as M4 V and M3.5 V, respectively.

Our spectra are not high enough resolution to be able to detect single- and double-lined spectroscopic binaries, however, we identify four targets which are potential white dwarf-M dwarf binaries. The spectra of KIC 07983929, KIC 09713959, KIC 09772829, and KIC 10064337 have excess flux toward blue wavelengths (Figure 6), which we attribute to a companion. Additionally, these spectra have similar spectral shapes to red-optical spectra of white dwarf-M dwarf binaries in the literature (e.g., Ren et al. 2014; Skinner et al. 2017). It is possible that the excess blue flux could be due to either improper flux calibration, slit losses, or atmospheric dispersion. Since all these binary candidates were observed using Hydra, we checked the spectra of other M dwarfs observed at the same time in the same field configuration and find no excess blue flux in these targets. Additionally, none of these targets were observed with the same fiber, and other targets observed with the same fiber in a different fiber configuration do not exhibit excess blue flux. We recommend additional spectroscopic observations of these targets at red and blue wavelengths to check that these effects are not from

instrument systematics, and to confirm our assessment that these systems are likely white dwarf-M dwarf binaries. Wang et al. (2014) and Kraus et al. (2016) find that close binary companions appear to suppress planet formation, and hence decrease planet occurrence rates for these systems. As such, we remove the eclipsing and candidate white dwarf-M dwarf binaries from our analysis of planet occurrence rates, reducing our sample to 551 stars.

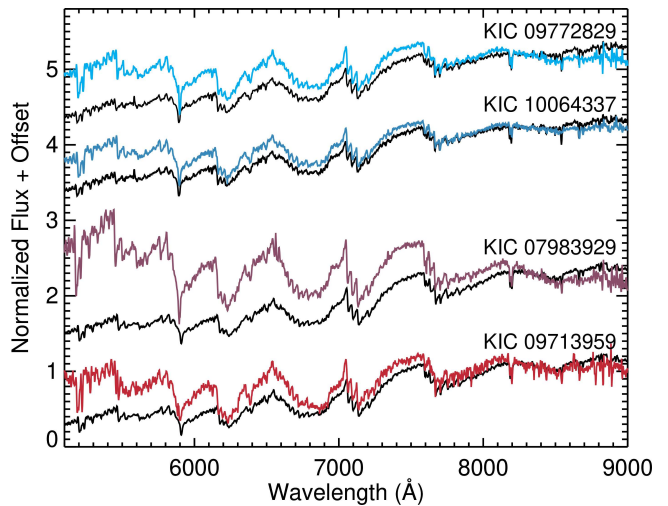


Figure 6. Four potential white dwarf-M dwarf binaries. KIC 09772829 and KIC 10064337 are compared an M2 V spectrum, and KIC 07983929 and KIC 09713959 are compared to an M3 V spectrum (black). Spectra are normalized to 8,350 Å.

4.3. *Gaia* Color Cuts and Binaries

We identify 61 targets with more than one source within $4''$ of the KIC coordinates, in which case we choose the target with the smallest difference in $G - K_p$ magnitudes. We also check if the M_{K_s} magnitudes (Section 3.1) are in the range we expect for an M dwarf ($4.6 \lesssim M_{K_s} \lesssim 9.8$; M15). Four targets for which we do not have spectra (KIC 10711066, KIC 10473048, KIC 06757650, and KIC 06029053) have *Gaia* coordinates $< 0''.4$ from the KIC coordinates, but have M_{K_s} magnitudes of 2.0, -1.6, -3.7, and 3.2, respectively. We discard these four sources from our analysis as they are likely non-M dwarfs, reducing our sample to 547 stars. Two spectroscopically observed targets, KIC 04545041 (M3.5 V) and KIC 03631048 (M4 V) have M_{K_s} of 4.06 and 4.45, respectively. Additionally, two photometrically classified targets, KIC 11196417 (M5 V) and KIC 10991155 (M4 V), have M_{K_s} of 4.53 and 4.56, respectively. For these four targets, we use their effective temperatures to determine radius since the M_{K_s} vs. R_* relationships do not extend to $M_{K_s} < 4.6$.

¹¹ <http://keplerebs.villanova.edu/>, as of April 2019

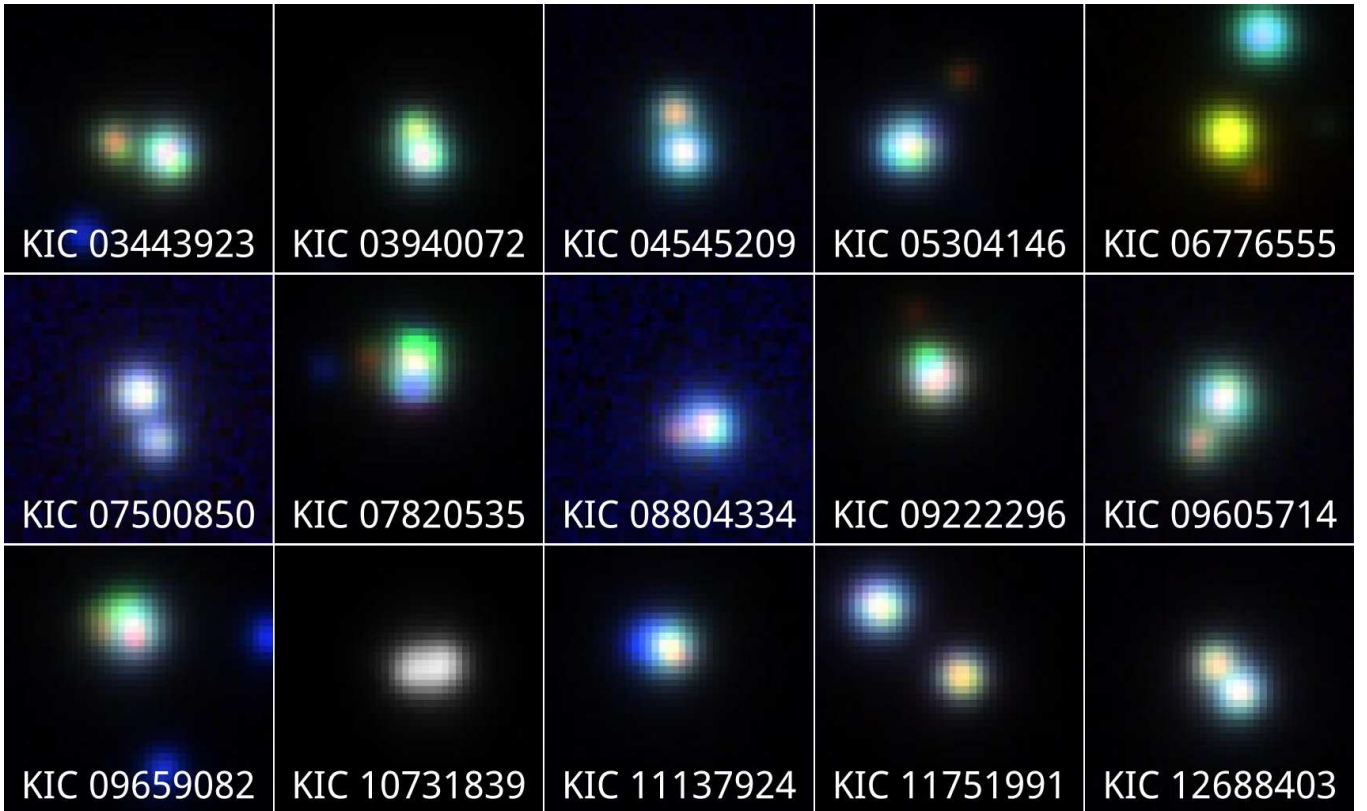


Figure 7. Probable binary stars sharing common proper motions and distances in the *Gaia* data. These $10''$ cutouts are stacked g , i , and y -band images from Pan-STARRS and are centered on the target coordinates from the NASA Exoplanet Archive. The image for KIC 10731839 is only g -band since it is saturated in the other filters.

Within the *Gaia* data, 15 targets have a nearby star with a similar distance and common proper motion, which we identify as probable binaries. In Figure 7 we show $10''$ cutout images of these 15 targets from the Panoramic Survey Telescope and Rapid Response System survey (Pan-STARRS, Chambers et al. 2016). We do not discard these stars in our analysis, since we use the $G - Kp$ color selection to identify our primary targets. In total, we have identified 21 binaries and binary candidates, which is 3.65% of our total sample. Duchêne & Kraus (2013) report a decreasing stellar multiplicity frequency with decreasing stellar mass, and estimate that $26 \pm 3\%$ of M dwarfs are in multiple systems. Winters et al. (2019) find an M dwarf multiplicity of $26.8 \pm 1.4\%$, and also note that lower mass M dwarfs have fewer companions than higher mass M dwarfs. We recognize that there are likely more unresolved binaries in our sample since we detect a $\sim 4\%$ binary fraction, much lower than the expected $\sim 27\%$, however, the assessment of the effect of binaries on planet occurrence rates is beyond the scope of this paper.

5. MID-TYPE M DWARF PLANETS

With our updated stellar properties in hand, we now turn to planets around mid-type M dwarfs. In our *Kepler* star sample, there are six planet systems containing 12 confirmed planets. We also include Kepler-1650 b, for which the host star has an $r - J$ color of 3.167, just missing our color cut. Muirhead et al. (2014) identify Kepler-1650 as an M3 V star from H and K -band spectra. Our optical spectrum of this target gives us a classification of M3.5 V. Spectra for all planet host stars are shown in Figure 8.

Additionally, there are four Kepler Objects of Interest (KOI) within our sample: KOI-959, KOI-5237, KOI-6705, and KOI-8012. Based on our spectra, KOI-959 (KIC 10002261), KOI-5327 (KIC 06776555), KOI-8012 (KIC 10452252) have spectral types of M3.5 V, M4 V, and M5 V, respectively. Using the spectral index typing system of Lépine et al. (2013), Gaidos et al. (2016a) report KOI-6705 (KIC 06423922) to be an M3.4 V star from a SNIFS optical spectrum.

Slawson et al. (2011) identify KOI-959 to be an eclipsing binary, which makes this planet candidate an astrophysical false positive. Additionally, Furlan et al. (2017) and Ziegler et al. (2018) find a nearby companion to KOI-959 at a separation of $\sim 0''.77$ using adap-

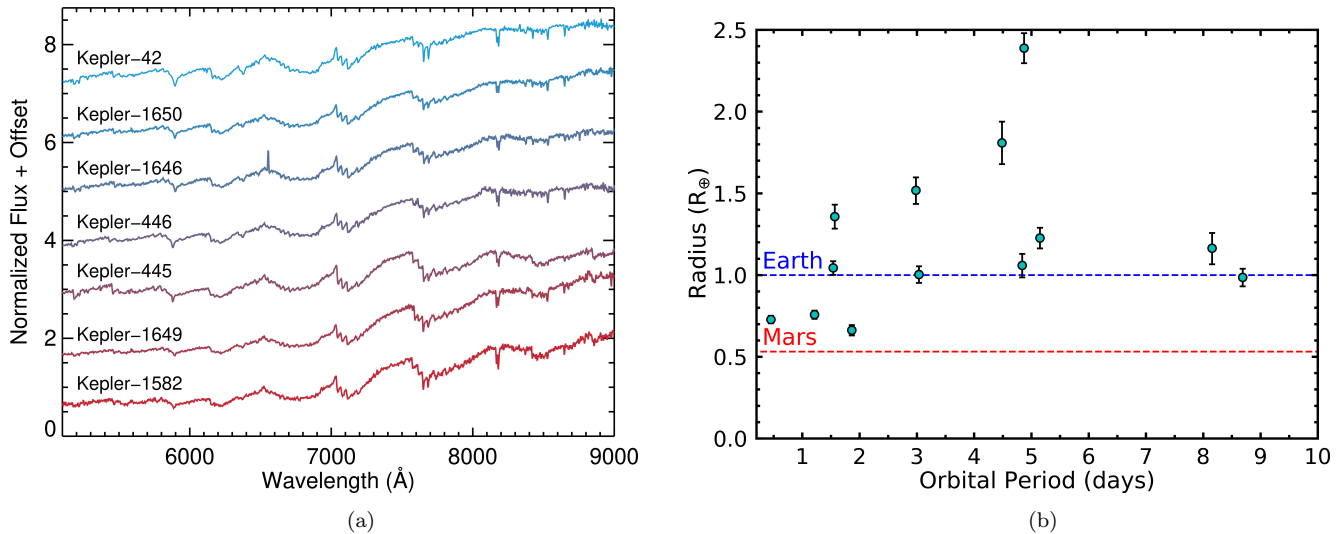


Figure 8. (a) Planet host spectra for *Kepler* mid-type M dwarfs, ordered by spectral type from M3 V (top) to M5 V (bottom). These are the first published optical spectra for Kepler-1646 (M4 Ve) and Kepler-1582 (M5 V). (b) Orbital period versus planet radius for *Kepler* mid-type M dwarfs. The planet radii have been updated using our new stellar radius measurements. The radii of Earth and Mars are shown for reference.

tive optics imaging. KOI-5327 is associated with three nearby companions at separations of $1''.88$, $3''.63$, and $3''.96$ (Ziegler et al. 2017; Furlan et al. 2017). The *Kepler* pipeline data validation report for this system shows an out-of-transit centroid offset of $2''.09$ (6.3σ), which might be due to the closest companion star. It is unclear which star the planet orbits, so we do not include this system in our analysis. Gaidos et al. (2016a) identify KOI-6705.01 as a likely false positive due to charge transfer inefficiency in a detector column on which a nearby eclipsing binary falls. Thompson et al. (2018) identify KOI-8012.01 as a Mercury-sized planet candidate in the habitable zone of its host star. Our reassessment of the radius of KOI-8012 places it at $0.43 R_{\oplus}$, which in turn increases the planet candidate radius to $0.83 R_{\oplus}$. We do not include this planet candidate in our analysis since the system parameters (e.g., period, semi-major axis) do not have reported uncertainties, which makes accurate analysis of this system difficult. Additionally, the *Kepler* light curve for KOI-8012 shows significant variability and extreme flare activity, which suggests that any planet candidates around this star could be astrophysical false positives.

Table 2 and Figure 8 show the confirmed planets around mid-type M dwarfs in the *Kepler* field. We note that all these planets are smaller than Neptune ($3.865 R_{\oplus}$) and have orbital periods shorter than 10 days. We update the planet parameters for all these systems based on our stellar radius and mass measure-

ments, and compute insolation flux S_p using:

$$\left(\frac{S_p}{S_{\oplus}}\right) = \left(\frac{L_{\star}}{L_{\odot}}\right) \left(\frac{AU}{a}\right)^2, \quad (4)$$

where $(L_{\star}/L_{\odot}) = (R_{\star}/R_{\odot})^2 (T_{\text{eff}}/T_{\odot})^4$ is the stellar luminosity, and a is the semi-major axis in AU, computed from Kepler’s third law using planet orbital period from the literature and our stellar masses. The planet with the lowest stellar irradiance in our sample is Kepler-1649 b, an Earth-sized planet ($R_p = 0.985 \pm 0.054 R_{\oplus}$) receiving nearly twice the stellar irradiation as Earth. The habitable zone definitions of Kopparapu et al. (2013) place this planet above the maximum greenhouse stellar irradiance limit.

6. PLANET OCCURRENCE RATE

With our updated stellar properties of 547 stars and a population of 13 planets around mid-type M dwarfs, we now have the critical pieces necessary to compute planet occurrence rates. We adopt the grid-based method (e.g., Howard et al. 2012; Dressing & Charbonneau 2013; Petigura et al. 2013) to compute planet occurrence rates, $f(R_p, P)$, which is the fraction of stars in a population (e.g., mid-type M dwarfs) that have planets with specific radii R_p and orbital periods P . Using the population of known planets around *Kepler* mid-type M dwarfs, we count the number of *Kepler* mid-type M dwarfs $N_{\star,i}$ around which the i^{th} known planet could have been detected with sufficient photometric precision

if it was at a transiting orbital inclination:

$$f(R_p, P) = \sum_{i=1}^{N_p} \frac{1/p_i}{N_{*,i}}, \quad (5)$$

where the sum is over the number of known planets N_p from the *Kepler* data within the specified planet radius and orbital period range. The probability p that planet i is in a transiting geometry, is defined as:

$$p_i = \left(\frac{R_{*,i} + R_p}{a_i} \right) \left(\frac{1 + e_i \sin \omega_i}{1 - e_i^2} \right), \quad (6)$$

where a_i is the semi-major axis of planet i , e_i is the eccentricity, and ω_i is the longitude of periastron (Winn 2010; Stevens & Gaudi 2013). Typically, $R_p \ll R_*$ and small planets on close-in orbits are nearly circular, which makes $p_i \approx R_{*,i}/a_i$. However, an Earth-sized planet around a mid-type M dwarf is between 2.5 and 7.5% of its host star diameter, which can have a small effect on the transit probability. Assuming circular orbits, we use:

$$p_i = \left(\frac{R_{*,i} + R_p}{a_i} \right). \quad (7)$$

We compute $N_{*,i}$ from the number of stars for which the S/N from the *Kepler* photometry is high enough that a known planet could be detected. The S/N is calculated by:

$$S/N = \frac{R_p^2/R_*^2}{\text{CDPP}_{\text{eff}}} \sqrt{\frac{t_{\text{obs}}}{P}}, \quad (8)$$

where CDPP_{eff} is the Combined Differential Photometric Precision over the duration of the transit, t_{obs} is the total time spent observing the star with *Kepler*, and P is the known planet orbital period (Muirhead et al. 2015). CDPP_{eff} , more precisely, is an estimate of white noise during a specific transit duration (Christiansen et al. 2012). For each star, we fit a power law to the CDPP values versus time for transits between 1.5 and 15 hours, and use this fit to determine CDPP_{eff} for each planet transit duration, t_{dur} . We compute t_{dur} for known planets using:

$$t_{\text{dur}} = \frac{P}{\pi} \sin^{-1} \left(\frac{\sqrt{(R_* + R_p)^2 - (bR_*)^2}}{a} \right), \quad (9)$$

where $b = a \cos \theta / R_*$ is the impact parameter with orbital inclination angle θ .

We use the linear ramp detection efficiency model from Mulders et al. (2015a), which was adapted from Fressin et al. (2013), where detection efficiency $f_{\text{eff}} = 0$ for $S/N \leq 6$, $f_{\text{eff}} = 1$ for $S/N > 12$, and $f_{\text{eff}} =$

$(S/N - 6)/6$ for $6 < S/N \leq 12$. The sum of the detection efficiencies, rounded to the nearest integer, then becomes $N_{*,i}$.

Our stellar selection criteria were chosen to isolate stars with a spectral type of M3 V and beyond, though we observed 40 stars with earlier spectral types. In our planet sample, we have identified the *Kepler* planets around M3 V to M5 V stars. For our planet occurrence rate calculations, we only consider the stars in this spectral type range.

6.1. Monte Carlo Analysis

The measured star and planet parameters found in Equations 7, 8, and 9 have uncertainties which contribute to the total uncertainty of the planet occurrence rate calculation. There is also spectral type uncertainty, which can move stars, including planet hosts, into or out of a spectral type bin. Additionally, due to our small planet sample size, we need to account for counting errors. In order to address these uncertainties we perform the following MC analysis. First, we address the ± 1 spectral type uncertainty by drawing a random number from a uniform distribution between -1 and 1 for each star in our sample and add those numbers to each spectral type. Second, we draw a number of planet detections N_p from a Poisson distribution with an expectation value (λ) equal to the detected planet sample size, similar to the method used in Silburt et al. (2015) and Gaidos et al. (2016b). For example, our total *Kepler* mid-type M dwarf planet sample size is 13, so we randomly draw a number from a Poisson distribution with $\lambda = 13$, then sample with replacement that number of planets from our mid-type M dwarf planet catalog to run the occurrence rate calculations. Next, for each parameter with an uncertainty measurement in Equations 7, 8, and 9, we generate 10^4 random samples from a Gaussian distribution and perform each calculation with these distributions. We also account for the effect of transit duration on S/N by assigning a random inclination angle to compute the impact parameter in Equation 9. We then run the results through Equation 5, and repeat this procedure 10^3 times for seven different bins: all mid-type M dwarfs (M3 V to M5.5 V), individual spectral types (M3 V to M3.5 V, M4 V to M4.5 V, and M5 V to M5.5 V), Earth-sized planets ($0.5 R_{\oplus} < R_p < 1.5 R_{\oplus}$), super-Earths ($1.5 R_{\oplus} < R_p < 2.5 R_{\oplus}$), and compact multiples.

The resulting planet occurrence rates and planet detection distributions are shown in Figure 9. The occurrence rate distributions all exhibit positive skew, highlighted by the box-and-whisker plots above each distribution. Due to our random selection of N_p from a

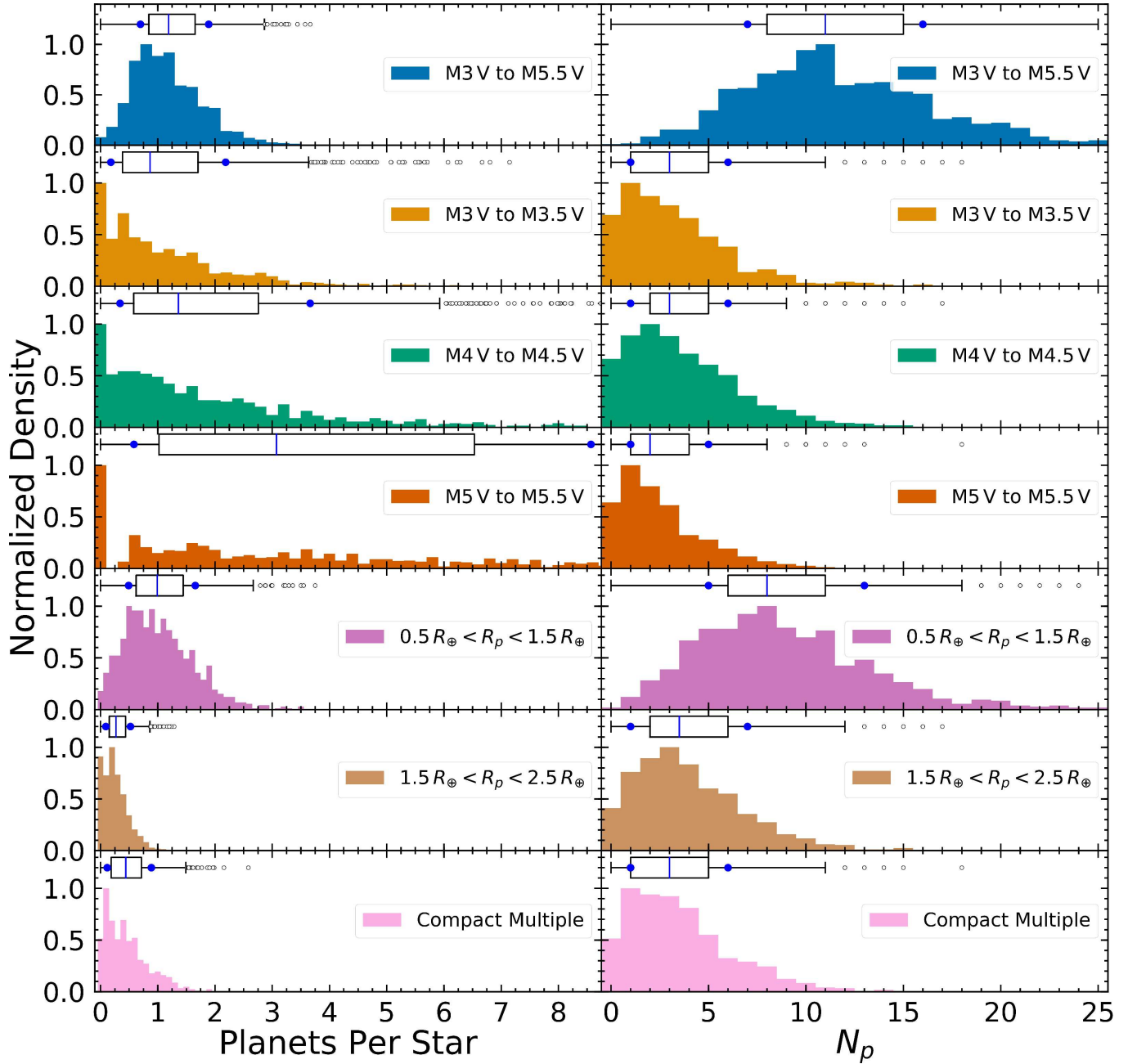


Figure 9. (Left) Planet occurrence rate distributions from our Monte Carlo analysis for different spectral type bins, planet radius bins, and for compact multiple systems. Above each distribution we give the corresponding box-and-whisker plot, which show the quartiles of each distribution. The 16th and 84th percentiles are shown as blue circles, and any outliers beyond $Q3 + 1.5 \times IQR$ are shown as open circles. The M5 V upper whisker extends to ~ 15 , however, we restrict the horizontal range to just beyond the 84th percentile of the M5 V distribution for clarity in the other plots. All of these plots are normalized such that the peak of each distribution is equal to one. (Right) Planet detection distributions from the planet occurrence rate Monte Carlo analysis and corresponding box-and-whisker plots.

Poisson distribution, an outcome of zero planets is possible, which results in a planet occurrence rate of zero. For our seven different bins, those with a smaller initial sample of planets are more likely to randomly draw zero planets. This effect is most prominent for the individual spectral type bins, which have prominent peaks at

zero for the planet occurrence rate. Even though the N_p distributions have a non-zero median, drawing zero planets will always result in an occurrence rate of zero, whereas drawing one or more planets can result in a different planet occurrence rate depending on the transit probability of the randomly selected planets and number

of stars from the MC calculation, effectively smoothing out other peaks. We report the results from the planet occurrence rate calculation in Table 1.

Table 1. Planet occurrence rates per spectral type, planet radius, and compact multiples for mid-type M dwarfs.

Range	Planets per star	N_p	$N_{*,i}$
M3 V to M5.5 V	$1.19^{+0.70}_{-0.49}$	11^{+5}_{-4}	412^{+8}_{-8}
M3 V to M3.5 V	$0.86^{+1.32}_{-0.68}$	3^{+3}_{-2}	95^{+8}_{-8}
M4 V to M4.5 V	$1.36^{+2.30}_{-1.02}$	3^{+3}_{-2}	92^{+9}_{-8}
M5 V to M5.5 V	$3.07^{+5.49}_{-2.49}$	2^{+3}_{-1}	37^{+5}_{-6}
$0.5 R_{\oplus} < R_p < 1.5 R_{\oplus}$	$0.99^{+0.66}_{-0.50}$	8^{+5}_{-3}	412^{+8}_{-9}
$1.5 R_{\oplus} < R_p < 2.5 R_{\oplus}$	$0.27^{+0.25}_{-0.18}$	4^{+3}_{-3}	412^{+7}_{-9}
Compact Multiple	$0.44^{+0.45}_{-0.33}$	3^{+3}_{-2}	411^{+8}_{-8}

NOTE—We report the median, 16th, and 84th percentiles of each distribution from 10^3 Monte Carlo trials.

7. DISCUSSION

For early-type M dwarfs with orbital periods between 0.5 and 10 days and planets with $0.5 R_{\oplus} < R_p < 2.5 R_{\oplus}$, DC15 derive a planet occurrence rate of $0.63^{+0.08}_{-0.06}$ planets per star. Similarly, Mulders et al. (2015b) compute a planet occurrence rate for M dwarfs in this range to be 0.53 planets per star. Our total occurrence rate for mid-type M dwarfs is approximately double that of DC15 and Mulders et al. (2015b) for early-type M dwarfs. We show a comparison of occurrence rates from our MC analysis to values from DC15 and Mulders et al. (2015b) in Figure 10. We also include in this figure the planet occurrence rates for stars of each spectral type F, G, and K from Mulders et al. (2015b). There is a clear trend of increasing planet occurrence toward later spectral types. If we take the median values of planet occurrence rates from our MC analysis, this suggests an increasing trend of small planets at short orbital periods toward later-type M dwarfs. We also find that a typical mid-type M dwarf will host a short period Earth-sized planet ($0.5 R_{\oplus} < R_p < 1.5 R_{\oplus}$), and larger planets are about four times less common.

We revise the planet occurrence rate for compact multiples around mid-type M dwarfs to be $0.44^{+0.45}_{-0.33}$. This value is computed following the same MC procedure, but only considers the detectability of the outermost planet in the multi-planet system. Our occurrence rate for compact multiples is consistent within 1σ to $0.21^{+0.07}_{-0.05}$ reported by Muirhead et al. (2015), though our median value is higher due to our revised stellar radii. Muirhead et al. (2015) assumed a uniform stellar radius of $0.2 R_{\odot}$, the peak of the radius distribution for these

stars in the *Kepler* Stellar Catalog. For low mass stars, Boyajian et al. (2012) found that evolutionary models, which were largely used to determine radii in the *Kepler* Stellar Catalog, under predict stellar radii. Our radius measurements have a median value of $0.33 R_{\odot}$, 58% larger than the median $0.21 R_{\odot}$ from the *Kepler* Stellar Catalog. The stellar radii reported in Gaidos et al. (2016b) were a significant improvement over those derived from evolutionary models, but they are still $\sim 20\%$ smaller than our measurements (Figure 4).

Ballard & Johnson (2016) assessed planet multiplicity among *Kepler* M dwarfs, and found that half of these systems contain five or more co-planar planets, while the other half are either single or multiple planet systems with large mutual planet inclinations. Of the seven confirmed *Kepler* mid-type M dwarf planet systems, three of them contain at least three planets, whereas the other four systems contain at least one planet. It is possible that all of these systems could contain additional non-transiting planets or planets that fall below the detection threshold of *Kepler*. The discovery of seven Earth-sized planets around the M8 V star TRAPPIST-1 shows that planet formation occurs through the end of the main sequence (Gillon et al. 2017), and supports both the increase in planet occurrence rates toward later spectral types and the large planet multiplicity from Ballard & Johnson (2016).

Thompson et al. (2018) note that pipeline detection efficiency, astrophysical reliability, and imperfect stellar information must all be taken into account for planet occurrence rate calculations. Pipeline detection efficiency has been computed for *Kepler* F, G, and K stars using pixel-level and flux-level transit injection (Christiansen et al. 2016; Christiansen 2017; Burke & Catanzarite 2017). DC15 performed their own pipeline detection efficiency for *Kepler* M dwarfs by injecting transit signals into light curves for all their target stars. For planets between $1 R_{\oplus}$ and $3 R_{\oplus}$ at orbital periods less than 10 days, their pipeline was able to recover between 80 and 90% of the injected transit signals. For planets below $1 R_{\oplus}$, recovery averaged 58%. Astrophysical reliability tests are used to determine whether or not an observed event is due to instrumental or stellar noise or other astrophysical events. Certain signals can mimic a planet transit (e.g., eclipsing binaries, background eclipsing binaries), so tools have been developed to automatically vet planet candidates (e.g., Robovetter, Thompson et al. 2018) and statistically validate planet candidates (e.g., *vespa*, Morton et al. 2016). Our work has addressed the third issue of imperfect stellar information, though we do take into account a simple linear ramp model of detection efficiency in our calculations.

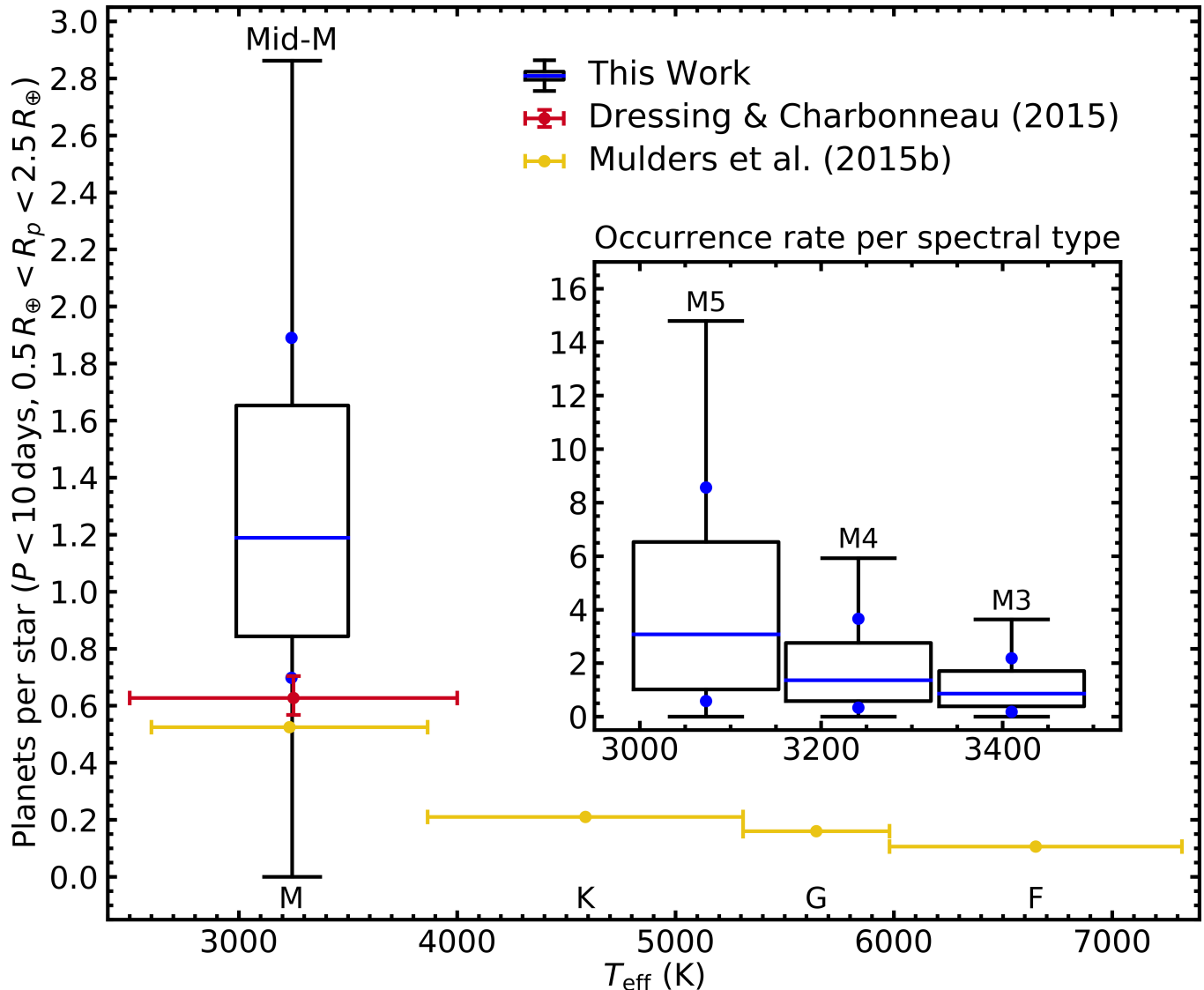


Figure 10. Planet occurrence rate as a function of stellar effective temperature for planets with orbital periods shorter than 10 days and radii between $0.5 R_{\oplus}$ and $2.5 R_{\oplus}$. The measurements from our Monte Carlo analysis are shown as box-and-whisker plots (see Figure 9), where the blue line indicates the median value, the blue dots are the 16th and 84th percentiles of the distributions, and the box width corresponds to the temperature uncertainty. The inset plot shows the planet occurrence rates for M3 V, M4 V, and M5 V, which show evidence for an increase of planet occurrence toward later M dwarfs.

We also note that Silburt et al. (2015) and Gaidos et al. (2016b) caution placing planets into discrete radius and period bins because it ignores information about the underlying planet distribution and will underestimate the planet occurrence rate. With a sample of only 13 planets, however, it is difficult to determine a practical planet distribution without making some assumptions. Additionally, accounting for small planet sample size dominates the error budget for our occurrence rate calculations.

From our *Kepler* planet occurrence rates, we can predict the number of planets in orbital periods less than 10 days around mid-type M dwarfs in the local neigh-

borhood. Stelzer et al. (2013) conducted a survey of UV and X-ray activity of M dwarfs within 10 parsecs of the Sun, in which they observed 159 M0 V through M8 V stars, and estimated that their volume-limited M dwarf sample was 90% complete. This sample includes 101 stars with spectral types between M3 V and M5.5 V, which means there are potentially 120^{+71}_{-49} small, short period planets around these nearby stars. So far, there have been 20 planets found around 9 of these nearby mid-type M dwarfs, all discovered via the radial velocity

technique¹². Of those 20 planets, 10 have orbital periods shorter than 10 days. The faintest mid-type M dwarf around which a planet has been detected using the radial velocity technique has a V -band magnitude of 12.22 (GJ 3323), and the smallest radial velocity amplitude for a planet detected around these stars is $1.06 \pm 0.15 \text{ m s}^{-1}$ (GJ 273 c, [Astudillo-Defru et al. 2017](#)). There are 51 nearby mid-type M dwarfs with V -band magnitudes less than 12.22. Our planet occurrence rates suggest there are 61_{-25}^{+35} small, short period planets around these stars. Since 10 of these planets have already been found, there may be around 50 additional planets orbiting nearby mid-type M dwarfs which could be detected with current radial velocity instruments (e.g., HARPS, [Pepe et al. 2011](#)), assuming the planets are massive enough to induce a 1 m s^{-1} signal. NEID and EXPRES aim to achieve even greater precision below 30 cm s^{-1} at optical wavelengths ([Halverson et al. 2016](#); [Jurgenson et al. 2016](#)). The Habitable Zone Planet Finder (HPF; [Mahadevan et al. 2012](#)) will specifically target mid- to late-type M dwarfs at near-infrared wavelengths, with a goal of 1 m s^{-1} precision. Recent commissioning observations with HPF have already achieved 1.3 m s^{-1} precision on Barnard’s Star ([Mahadevan et al. 2018](#)).

Since the original *Kepler* mission was designed to detect Earth-like planets around Sun-like stars, less emphasis was placed on low-mass stars. The *K2* mission ([Howell et al. 2014](#)), however, was well suited for detecting planets around the latest type stars along the ecliptic plane, and has already produced dozens of confirmed and candidate planets around M dwarfs, opening up another rich data set to expand this planet occurrence rate study. The *K2* M Dwarf Project (PIs Schleider, J.; Crossfield, I.; Dressing, C.) alone has over 25,000 targets in *K2* Campaigns 4 through 19, about five times larger than the number of M dwarfs observed with *Kepler*. The ground based survey MEarth ([Nutzman & Charbonneau 2008](#)) is surveying M dwarfs for planets, and the Search for habitable Planets EClipping ULtra-cOOl Stars (SPECULOOS; [Burdanov et al. 2017](#)) is starting to search for planets around 1,000 late-type M dwarfs and brown dwarfs. Since small, short period planets are more prevalent around smaller stars, these surveys should be fruitful. The recently launched *TESS* mission is also expected to find 500 to 1,000 planets around bright M dwarfs across the entire night sky ([Barclay et al. 2018](#); [Ballard 2018](#)). [Barclay et al. \(2018\)](#) predicted that 54 planets will be found with or-

bitual periods less than 10 days around bright ($K_S < 10$) mid-type M dwarfs, assuming the occurrence rates of [DC15](#). Based on our occurrence rates, we expect a more optimistic *TESS* yield of ~ 100 planets around bright mid-type M dwarfs.

8. ACKNOWLEDGEMENTS

We would like to thank WIYN observing assistants Amy Robertson, Anthony Paat, Christian Soto, Dave Summers, Doug Williams, Karen Butler, and Malanka Riabokin, DCT telescope operators Andrew Hayslip, Heidi Larson, Jason Sanborn, and Teznie Pugh, and IRTF telescope operators Brian Cabreira, Dave Griep, Eric Volquardsen, Greg Osterman, and Tony Matulonis. We would also like to thank NOAO observing support scientists Daryl Willmarth, Dianne Harmer, Mark Everett, and Susan Ridgway. K. Hardegree-Ullman would like to thank Adam Schneider and Wayne Oswald for conducting some of the observations herein at the DCT and WIYN, and Courtney Dressing, Gijs Mulders, and Jon Zink for informative discussions regarding planet occurrence rates and statistics.

Data presented herein were obtained at the WIYN Observatory from telescope time allocated to NN-EXPLORE through the scientific partnership of the National Aeronautics and Space Administration, the National Science Foundation, and the National Optical Astronomy Observatory. This work was supported by a NASA WIYN PI Data Award, administered by the NASA Exoplanet Science Institute.

These results made use of the Discovery Channel Telescope at Lowell Observatory. Lowell is a private, non-profit institution dedicated to astrophysical research and public appreciation of astronomy and operates the DCT in partnership with Boston University, the University of Maryland, the University of Toledo, Northern Arizona University and Yale University. The upgrade of the DeVeny optical spectrograph has been funded by a generous grant from John and Ginger Giovale.

Guoshoujing Telescope (the Large Sky Area Multi-Object Fiber Spectroscopic Telescope LAMOST) is a National Major Scientific Project built by the Chinese Academy of Sciences. Funding for the project has been provided by the National Development and Reform Commission. LAMOST is operated and managed by the National Astronomical Observatories, Chinese Academy of Sciences.

This research has made use of the NASA Exoplanet Archive, which is operated by the California Institute of Technology, under contract with the National Aeronautics and Space Administration under the Exoplanet Exploration Program.

¹² <https://exoplanetarchive.ipac.caltech.edu/cgi-bin/TblView/nph-tblView.pl?tblname=exoplanets&tblcol=ra&tblrow=1> as of April 2019

This work has made use of data from the European Space Agency (ESA) mission *Gaia* (<https://www.cosmos.esa.int/gaia>), processed by the *Gaia* Data Processing and Analysis Consortium (DPAC, <https://www.cosmos.esa.int/web/gaia/dpac/consortium>). Funding for the DPAC has been provided by national institutions, in particular the institutions participating in the *Gaia* Multilateral Agreement.

This work made use of the *gaia-kepler.fun* crossmatch database created by Megan Bedell.

The Pan-STARRS1 Surveys (PS1) and the PS1 public science archive have been made possible through contributions by the Institute for Astronomy, the University of Hawaii, the Pan-STARRS Project Office, the Max-Planck Society and its participating institutes, the Max Planck Institute for Astronomy, Heidelberg and the Max Planck Institute for Extraterrestrial Physics, Garching, The Johns Hopkins University, Durham University, the University of Edinburgh, the Queen’s University Belfast, the Harvard-Smithsonian Center for Astrophysics, the Las Cumbres Observatory Global Telescope Network Incorporated, the National Central University of Tai-

wan, the Space Telescope Science Institute, the National Aeronautics and Space Administration under Grant No. NNX08AR22G issued through the Planetary Science Division of the NASA Science Mission Directorate, the National Science Foundation Grant No. AST-1238877, the University of Maryland, Eotvos Lorand University (ELTE), the Los Alamos National Laboratory, and the Gordon and Betty Moore Foundation.

The authors wish to recognize and acknowledge the very significant cultural role and reverence that the summit of Maunakea has always had within the indigenous Hawaiian community. We are most fortunate to have the opportunity to conduct observations from this mountain.

Facilities: WIYN (Hydra), DCT (DeVeny), IRTF (SpeX), NASA Exoplanet Archive

Software: dustmaps (Green et al. 2018), IDL Astronomy User’s Library (Landsman 1993), IRAF (Tody 1986, 1993), numpy (Oliphant 2015), scikit-learn (Pedregosa et al. 2011), Spextool (Cushing et al. 2004), xtellcor (Vacca et al. 2003)

REFERENCES

- Abdul-Masih, M., Prša, A., Conroy, K., et al. 2016, *AJ*, 151, 101, doi: [10.3847/0004-6256/151/4/101](https://doi.org/10.3847/0004-6256/151/4/101)
- Angelo, I., Rowe, J. F., Howell, S. B., et al. 2017, *AJ*, 153, 162, doi: [10.3847/1538-3881/aa615f](https://doi.org/10.3847/1538-3881/aa615f)
- Astudillo-Defru, N., Forveille, T., Bonfils, X., et al. 2017, *A&A*, 602, A88, doi: [10.1051/0004-6361/201630153](https://doi.org/10.1051/0004-6361/201630153)
- Bailer-Jones, C. A. L. 2015, *PASP*, 127, 994, doi: [10.1086/683116](https://doi.org/10.1086/683116)
- Bailer-Jones, C. A. L., Rybizki, J., Fouesneau, M., Mantelet, G., & Andrae, R. 2018, ArXiv e-prints. <https://arxiv.org/abs/1804.10121>
- Ballard, S. 2018, arXiv e-prints, arXiv:1801.04949. <https://arxiv.org/abs/1801.04949>
- Ballard, S., & Johnson, J. A. 2016, *ApJ*, 816, 66, doi: [10.3847/0004-637X/816/2/66](https://doi.org/10.3847/0004-637X/816/2/66)
- Barclay, T., Pepper, J., & Quintana, E. V. 2018, ArXiv e-prints. <https://arxiv.org/abs/1804.05050>
- Barden, S. C., Armandroff, T., Muller, G., et al. 1994, in *Proc. SPIE*, Vol. 2198, *Instrumentation in Astronomy VIII*, ed. D. L. Crawford & E. R. Craine, 87–97
- Batalha, N. M., Borucki, W. J., Koch, D. G., et al. 2010, *ApJL*, 713, L109, doi: [10.1088/2041-8205/713/2/L109](https://doi.org/10.1088/2041-8205/713/2/L109)
- Berger, T. A., Huber, D., Gaidos, E., & van Saders, J. L. 2018, ArXiv e-prints. <https://arxiv.org/abs/1805.00231>
- Bochanski, J. J., Hawley, S. L., Covey, K. R., et al. 2010, *AJ*, 139, 2679, doi: [10.1088/0004-6256/139/6/2679](https://doi.org/10.1088/0004-6256/139/6/2679)
- Bochanski, J. J., West, A. A., Hawley, S. L., & Covey, K. R. 2007, *AJ*, 133, 531, doi: [10.1086/510240](https://doi.org/10.1086/510240)
- Borucki, W. J., Koch, D., Basri, G., et al. 2010, *Science*, 327, 977, doi: [10.1126/science.1185402](https://doi.org/10.1126/science.1185402)
- Boyajian, T. S., von Braun, K., van Belle, G., et al. 2012, *ApJ*, 757, 112, doi: [10.1088/0004-637X/757/2/112](https://doi.org/10.1088/0004-637X/757/2/112)
- Brown, T. M., Latham, D. W., Everett, M. E., & Esquerdo, G. A. 2011, *AJ*, 142, 112, doi: [10.1088/0004-6256/142/4/112](https://doi.org/10.1088/0004-6256/142/4/112)
- Burdanov, A., Delrez, L., Gillon, M., et al. 2017, *SPECULOOS Exoplanet Search and Its Prototype on TRAPPIST* (Springer), 130
- Burke, C. J., & Catanzarite, J. 2017, *Planet Detection Metrics: Per-Target Flux-Level Transit Injection Tests of TPS for Data Release 25*, Tech. rep., NASA
- Chambers, K. C., Magnier, E. A., Metcalfe, N., et al. 2016, ArXiv e-prints. <https://arxiv.org/abs/1612.05560>
- Christiansen, J. L. 2017, *Planet Detection Metrics: Pixel-Level Transit Injection Tests of Pipeline Detection Efficiency for Data Release 25*, Tech. rep., NASA
- Christiansen, J. L., Jenkins, J. M., Caldwell, D. A., et al. 2012, *PASP*, 124, 1279, doi: [10.1086/668847](https://doi.org/10.1086/668847)
- Christiansen, J. L., Clarke, B. D., Burke, C. J., et al. 2016, *ApJ*, 828, 99, doi: [10.3847/0004-637X/828/2/99](https://doi.org/10.3847/0004-637X/828/2/99)

- Cui, X.-Q., Zhao, Y.-H., Chu, Y.-Q., et al. 2012, *Research in Astronomy and Astrophysics*, 12, 1197, doi: [10.1088/1674-4527/12/9/003](https://doi.org/10.1088/1674-4527/12/9/003)
- Cushing, M. C., Rayner, J. T., & Vacca, W. D. 2005, *ApJ*, 623, 1115, doi: [10.1086/428040](https://doi.org/10.1086/428040)
- Cushing, M. C., Vacca, W. D., & Rayner, J. T. 2004, *PASP*, 116, 362, doi: [10.1086/382907](https://doi.org/10.1086/382907)
- Dotter, A., Chaboyer, B., Jevremović, D., et al. 2008, *ApJS*, 178, 89, doi: [10.1086/589654](https://doi.org/10.1086/589654)
- Dressing, C. D., & Charbonneau, D. 2013, *ApJ*, 767, 95, doi: [10.1088/0004-637X/767/1/95](https://doi.org/10.1088/0004-637X/767/1/95)
- . 2015, *ApJ*, 807, 45, doi: [10.1088/0004-637X/807/1/45](https://doi.org/10.1088/0004-637X/807/1/45)
- Duchêne, G., & Kraus, A. 2013, *ARA&A*, 51, 269, doi: [10.1146/annurev-astro-081710-102602](https://doi.org/10.1146/annurev-astro-081710-102602)
- Evans, D. W., Riello, M., De Angeli, F., et al. 2018, *ArXiv e-prints*. <https://arxiv.org/abs/1804.09368>
- Fressin, F., Torres, G., Charbonneau, D., et al. 2013, *ApJ*, 766, 81, doi: [10.1088/0004-637X/766/2/81](https://doi.org/10.1088/0004-637X/766/2/81)
- Furlan, E., Ciardi, D. R., Everett, M. E., et al. 2017, *AJ*, 153, 71, doi: [10.3847/1538-3881/153/2/71](https://doi.org/10.3847/1538-3881/153/2/71)
- Gaia Collaboration, Brown, A. G. A., Vallenari, A., et al. 2018, *ArXiv e-prints*. <https://arxiv.org/abs/1804.09365>
- Gaia Collaboration, Prusti, T., de Bruijne, J. H. J., et al. 2016, *A&A*, 595, doi: [10.1051/0004-6361/201629272](https://doi.org/10.1051/0004-6361/201629272)
- Gaidos, E. 2013, *ApJ*, 770, 90, doi: [10.1088/0004-637X/770/2/90](https://doi.org/10.1088/0004-637X/770/2/90)
- Gaidos, E., Mann, A. W., & Ansdell, M. 2016a, *ApJ*, 817, 50, doi: [10.3847/0004-637X/817/1/50](https://doi.org/10.3847/0004-637X/817/1/50)
- Gaidos, E., Mann, A. W., Kraus, A. L., & Ireland, M. 2016b, *MNRAS*, 457, 2877, doi: [10.1093/mnras/stw097](https://doi.org/10.1093/mnras/stw097)
- Gillon, M., Triaud, A. H. M. J., Demory, B.-O., et al. 2017, *Nature*, 542, 456, doi: [10.1038/nature21360](https://doi.org/10.1038/nature21360)
- Green, G. M., Schlafly, E. F., Finkbeiner, D., et al. 2018, *ArXiv e-prints*. <https://arxiv.org/abs/1801.03555>
- Halverson, S., Terrien, R., Mahadevan, S., et al. 2016, in *Proc. SPIE*, Vol. 9908, *Ground-based and Airborne Instrumentation for Astronomy VI*, 99086P
- Henry, T. J., Jao, W.-C., Subasavage, J. P., et al. 2006, *AJ*, 132, 2360, doi: [10.1086/508233](https://doi.org/10.1086/508233)
- Howard, A. W., Marcy, G. W., Bryson, S. T., et al. 2012, *ApJS*, 201, 15, doi: [10.1088/0067-0049/201/2/15](https://doi.org/10.1088/0067-0049/201/2/15)
- Howell, S. B., Sobek, C., Haas, M., et al. 2014, *PASP*, 126, 398, doi: [10.1086/676406](https://doi.org/10.1086/676406)
- Huber, D., Silva Aguirre, V., Matthews, J. M., et al. 2014, *ApJS*, 211, 2, doi: [10.1088/0067-0049/211/1/2](https://doi.org/10.1088/0067-0049/211/1/2)
- Jurgenson, C., Fischer, D., McCracken, T., et al. 2016, in *Proc. SPIE*, Vol. 9908, *Ground-based and Airborne Instrumentation for Astronomy VI*, 99086T
- Kirk, B., Conroy, K., Prša, A., et al. 2016, *AJ*, 151, 68, doi: [10.3847/0004-6256/151/3/68](https://doi.org/10.3847/0004-6256/151/3/68)
- Kirkpatrick, J. D., Henry, T. J., & McCarthy, Jr., D. W. 1991, *ApJS*, 77, 417, doi: [10.1086/191611](https://doi.org/10.1086/191611)
- Kopparapu, R. K., Ramirez, R., Kasting, J. F., et al. 2013, *ApJ*, 765, 131, doi: [10.1088/0004-637X/765/2/131](https://doi.org/10.1088/0004-637X/765/2/131)
- Kraus, A. L., Ireland, M. J., Huber, D., Mann, A. W., & Dupuy, T. J. 2016, *AJ*, 152, 8, doi: [10.3847/0004-6256/152/1/8](https://doi.org/10.3847/0004-6256/152/1/8)
- Landsman, W. B. 1993, in *Astronomical Society of the Pacific Conference Series*, Vol. 52, *Astronomical Data Analysis Software and Systems II*, ed. R. J. Hanisch, R. J. V. Brissenden, & J. Barnes, 246
- Lépine, S., Hilton, E. J., Mann, A. W., et al. 2013, *AJ*, 145, 102, doi: [10.1088/0004-6256/145/4/102](https://doi.org/10.1088/0004-6256/145/4/102)
- Mahadevan, S., Ramsey, L., Bender, C., et al. 2012, in *Ground-based and Airborne Instrumentation for Astronomy IV*, Vol. 8446, 84461S
- Mahadevan, S., Anderson, T., Balderrama, E., et al. 2018, in *SPIE Astronomical Telescopes + Instrumentation*, Vol. 10702. <https://doi.org/10.1117/12.2313835>
- Mann, A. W., Brewer, J. M., Gaidos, E., Lépine, S., & Hilton, E. J. 2013a, *AJ*, 145, 52, doi: [10.1088/0004-6256/145/2/52](https://doi.org/10.1088/0004-6256/145/2/52)
- Mann, A. W., Deacon, N. R., Gaidos, E., et al. 2014, *AJ*, 147, 160, doi: [10.1088/0004-6256/147/6/160](https://doi.org/10.1088/0004-6256/147/6/160)
- Mann, A. W., Feiden, G. A., Gaidos, E., Boyajian, T., & von Braun, K. 2015, *ApJ*, 804, 64, doi: [10.1088/0004-637X/804/1/64](https://doi.org/10.1088/0004-637X/804/1/64)
- Mann, A. W., Gaidos, E., & Ansdell, M. 2013b, *ApJ*, 779, 188, doi: [10.1088/0004-637X/779/2/188](https://doi.org/10.1088/0004-637X/779/2/188)
- Mann, A. W., Gaidos, E., Lépine, S., & Hilton, E. J. 2012, *ApJ*, 753, 90, doi: [10.1088/0004-637X/753/1/90](https://doi.org/10.1088/0004-637X/753/1/90)
- Mann, A. W., Dupuy, T., Muirhead, P. S., et al. 2017, *AJ*, 153, 267, doi: [10.3847/1538-3881/aa7140](https://doi.org/10.3847/1538-3881/aa7140)
- Mann, A. W., Dupuy, T., Kraus, A. L., et al. 2019, *ApJ*, 871, 63, doi: [10.3847/1538-4357/aaf3bc](https://doi.org/10.3847/1538-4357/aaf3bc)
- Martín, E. L., Cabrera, J., Martioli, E., Solano, E., & Tata, R. 2013, *A&A*, 555, A108, doi: [10.1051/0004-6361/201321186](https://doi.org/10.1051/0004-6361/201321186)
- Mathur, S., Huber, D., Batalha, N. M., et al. 2017, *ApJS*, 229, 30, doi: [10.3847/1538-4365/229/2/30](https://doi.org/10.3847/1538-4365/229/2/30)
- Merrill, P. W. 1922, *ApJ*, 56, 457, doi: [10.1086/142716](https://doi.org/10.1086/142716)
- . 1923, *Publications of the Astronomical Society of the Pacific*, 35, 217, doi: [10.1086/123312](https://doi.org/10.1086/123312)
- Morton, T. D., Bryson, S. T., Coughlin, J. L., et al. 2016, *ApJ*, 822, 86, doi: [10.3847/0004-637X/822/2/86](https://doi.org/10.3847/0004-637X/822/2/86)
- Muirhead, P. S., Hamren, K., Schlawin, E., et al. 2012, *ApJL*, 750, L37, doi: [10.1088/2041-8205/750/2/L37](https://doi.org/10.1088/2041-8205/750/2/L37)
- Muirhead, P. S., Becker, J., Feiden, G. A., et al. 2014, *ApJS*, 213, 5, doi: [10.1088/0067-0049/213/1/5](https://doi.org/10.1088/0067-0049/213/1/5)

- Muirhead, P. S., Mann, A. W., Vanderburg, A., et al. 2015, *ApJ*, 801, 18, doi: [10.1088/0004-637X/801/1/18](https://doi.org/10.1088/0004-637X/801/1/18)
- Mulders, G. D., Pascucci, I., & Apai, D. 2015a, *ApJ*, 798, 112, doi: [10.1088/0004-637X/798/2/112](https://doi.org/10.1088/0004-637X/798/2/112)
- . 2015b, *ApJ*, 814, 130, doi: [10.1088/0004-637X/814/2/130](https://doi.org/10.1088/0004-637X/814/2/130)
- Nutzman, P., & Charbonneau, D. 2008, *PASP*, 120, 317, doi: [10.1086/533420](https://doi.org/10.1086/533420)
- Oliphant, T. E. 2015, *Guide to NumPy*, 2nd edn. (USA: CreateSpace Independent Publishing Platform)
- Pecaut, M. J., & Mamajek, E. E. 2013, *ApJS*, 208, 9, doi: [10.1088/0067-0049/208/1/9](https://doi.org/10.1088/0067-0049/208/1/9)
- Pedregosa, F., Varoquaux, G., Gramfort, A., et al. 2011, *Journal of Machine Learning Research*, 12, 2825
- Pepe, F., Lovis, C., Ségransan, D., et al. 2011, *A&A*, 534, A58, doi: [10.1051/0004-6361/201117055](https://doi.org/10.1051/0004-6361/201117055)
- Petigura, E. A., Howard, A. W., & Marcy, G. W. 2013, *Proceedings of the National Academy of Science*, 110, 19273, doi: [10.1073/pnas.1319909110](https://doi.org/10.1073/pnas.1319909110)
- Rajpurohit, A. S., Reylé, C., Allard, F., et al. 2013, *A&A*, 556, A15, doi: [10.1051/0004-6361/201321346](https://doi.org/10.1051/0004-6361/201321346)
- Rayner, J. T., Cushing, M. C., & Vacca, W. D. 2009, *ApJS*, 185, 289, doi: [10.1088/0067-0049/185/2/289](https://doi.org/10.1088/0067-0049/185/2/289)
- Rayner, J. T., Toomey, D. W., Onaka, P. M., et al. 2003, *PASP*, 115, 362, doi: [10.1086/367745](https://doi.org/10.1086/367745)
- Reid, I. N., Hawley, S. L., & Gizis, J. E. 1995, *AJ*, 110, 1838, doi: [10.1086/117655](https://doi.org/10.1086/117655)
- Ren, J. J., Rebassa-Mansergas, A., Luo, A. L., et al. 2014, *A&A*, 570, A107, doi: [10.1051/0004-6361/201423689](https://doi.org/10.1051/0004-6361/201423689)
- Schwab, C., Rakich, A., Gong, Q., et al. 2016, in *Proc. SPIE*, Vol. 9908, Ground-based and Airborne Instrumentation for Astronomy VI, 99087H
- Ségransan, D., Kervella, P., Forveille, T., & Queloz, D. 2003, *A&A*, 397, L5, doi: [10.1051/0004-6361:20021714](https://doi.org/10.1051/0004-6361:20021714)
- Silburt, A., Gaidos, E., & Wu, Y. 2015, *ApJ*, 799, 180, doi: [10.1088/0004-637X/799/2/180](https://doi.org/10.1088/0004-637X/799/2/180)
- Skinner, J. N., Morgan, D. P., West, A. A., Lépine, S., & Thorstensen, J. R. 2017, *AJ*, 154, 118, doi: [10.3847/1538-3881/aa83b5](https://doi.org/10.3847/1538-3881/aa83b5)
- Skopal, A. 2005, *A&A*, 440, 995, doi: [10.1051/0004-6361:20034262](https://doi.org/10.1051/0004-6361:20034262)
- Skrutskie, M. F., Cutri, R. M., Stiening, R., et al. 2006, *AJ*, 131, 1163, doi: [10.1086/498708](https://doi.org/10.1086/498708)
- Slawson, R. W., Prša, A., Welsh, W. F., et al. 2011, *AJ*, 142, 160, doi: [10.1088/0004-6256/142/5/160](https://doi.org/10.1088/0004-6256/142/5/160)
- Stelzer, B., Marino, A., Micela, G., López-Santiago, J., & Liefke, C. 2013, *MNRAS*, 431, 2063, doi: [10.1093/mnras/stt225](https://doi.org/10.1093/mnras/stt225)
- Stevens, D. J., & Gaudi, B. S. 2013, *PASP*, 125, 933, doi: [10.1086/672572](https://doi.org/10.1086/672572)
- Thompson, S. E., Coughlin, J. L., Hoffman, K., et al. 2018, *ApJS*, 235, 38, doi: [10.3847/1538-4365/aab4f9](https://doi.org/10.3847/1538-4365/aab4f9)
- Tody, D. 1986, in *Proc. SPIE*, Vol. 627, Instrumentation in astronomy VI, ed. D. L. Crawford, 733
- Tody, D. 1993, in *Astronomical Society of the Pacific Conference Series*, Vol. 52, Astronomical Data Analysis Software and Systems II, ed. R. J. Hanisch, R. J. V. Brissenden, & J. Barnes, 173
- Vacca, W. D., Cushing, M. C., & Rayner, J. T. 2003, *PASP*, 115, 389, doi: [10.1086/346193](https://doi.org/10.1086/346193)
- von Braun, K., Boyajian, T. S., van Belle, G. T., et al. 2014, *MNRAS*, 438, 2413, doi: [10.1093/mnras/stt2360](https://doi.org/10.1093/mnras/stt2360)
- Wang, J., Fischer, D. A., Xie, J.-W., & Ciardi, D. R. 2014, *ApJ*, 791, 111, doi: [10.1088/0004-637X/791/2/111](https://doi.org/10.1088/0004-637X/791/2/111)
- West, A. A., Morgan, D. P., Bochanski, J. J., et al. 2011, *AJ*, 141, 97, doi: [10.1088/0004-6256/141/3/97](https://doi.org/10.1088/0004-6256/141/3/97)
- Winn, J. N. 2010, *Exoplanet Transits and Occultations* (University of Arizona Press), 55–77
- Winters, J. G., Henry, T. J., Jao, W.-C., et al. 2019, *arXiv e-prints*, arXiv:1901.06364, <https://arxiv.org/abs/1901.06364>
- York, D. G., Adelman, J., Anderson, Jr., J. E., et al. 2000, *AJ*, 120, 1579, doi: [10.1086/301513](https://doi.org/10.1086/301513)
- Ziegler, C., Law, N. M., Morton, T., et al. 2017, *AJ*, 153, 66, doi: [10.3847/1538-3881/153/2/66](https://doi.org/10.3847/1538-3881/153/2/66)
- Ziegler, C., Law, N. M., Baranec, C., et al. 2018, *AJ*, 155, 161, doi: [10.3847/1538-3881/aab042](https://doi.org/10.3847/1538-3881/aab042)

Table 2. Kepler Mid-Type M Dwarf Planets

Planet Name	Host Type (This Work)	R_\star (R_\odot)	R_p (R_\oplus)	a/R_\star	Period (days)	t_{dur} (hours)	Transit Probability	S_p (S_\oplus)	References
Kepler-42 b	M3 V	0.174 ± 0.005	0.757 ± 0.025	$14.46^{+0.43}_{-0.40}$	$1.2137706 \pm 2.4 \times 10^{-7}$	0.57 ± 0.04	0.0719 ± 0.0021	$26.86^{+3.31}_{-3.08}$	2
Kepler-42 c			0.727 ± 0.023	$7.49^{+0.23}_{-0.21}$	$0.45328731 \pm 5.0 \times 10^{-8}$	0.44 ± 0.03	0.1385 ± 0.0041	$99.78^{+12.16}_{-11.26}$	2
Kepler-42 d			0.662 ± 0.032	$19.26^{+0.59}_{-0.54}$	$1.86511236 \pm 7.3 \times 10^{-7}$	0.56 ± 0.09	0.0537 ± 0.0016	$15.13^{+1.88}_{-1.75}$	2
Kepler-1650 b	M3.5 V	0.364 ± 0.010	1.044 ± 0.042	$10.88^{+0.34}_{-0.31}$	$1.53818001 \pm 1.5 \times 10^{-6}$	1.05 ± 0.11	0.0942 ± 0.0028	$42.67^{+5.59}_{-4.88}$	2
Kepler-1646 b	M4 Ve	0.374 ± 0.011	1.809 ± 0.129	$21.86^{+0.71}_{-0.65}$	$4.48558383 \pm 1.1 \times 10^{-5}$	1.53 ± 0.07	0.0478 ± 0.0015	$9.57^{+1.29}_{-1.11}$	3
Kepler-446 b	M4 V	0.217 ± 0.006	1.357 ± 0.073	$14.94^{+0.46}_{-0.44}$	$1.565409 \pm 3.3 \times 10^{-6}$	0.67 ± 0.09	0.0708 ± 0.0022	$20.62^{+2.62}_{-2.50}$	4
Kepler-446 c			1.003 ± 0.051	$23.23^{+0.71}_{-0.68}$	$3.036179 \pm 5.5 \times 10^{-6}$	0.96 ± 0.10	0.0449 ± 0.0014	$8.47^{+1.11}_{-1.00}$	4
Kepler-446 d			1.227 ± 0.063	$33.02^{+1.03}_{-0.95}$	$5.148921 \pm 2.2 \times 10^{-5}$	0.93 ± 0.13	0.0318 ± 0.0010	$4.18^{+0.56}_{-0.49}$	4
Kepler-445 b	M4.5 V	0.305 ± 0.009	1.519 ± 0.079	$18.63^{+0.59}_{-0.57}$	$2.9841664 \pm 9.1 \times 10^{-6}$	1.27 ± 0.04	0.0561 ± 0.0018	$11.87^{+1.62}_{-1.43}$	2, 4
Kepler-445 c			2.390 ± 0.092	$25.82^{+0.83}_{-0.79}$	$4.87122714 \pm 6.3 \times 10^{-6}$	1.54 ± 0.05	0.0415 ± 0.0013	$6.17^{+0.83}_{-0.73}$	2, 4
Kepler-445 d			1.167 ± 0.098	$36.38^{+1.17}_{-1.10}$	$8.15272856 \pm 6.7 \times 10^{-5}$	1.75 ± 0.06	0.0284 ± 0.0009	$3.11^{+0.42}_{-0.38}$	2, 4
Kepler-1649 b	M5 V	0.231 ± 0.007	0.985 ± 0.054	$45.02^{+1.42}_{-1.36}$	$8.68909 \pm 2.4 \times 10^{-5}$	1.38 ± 0.27	0.0231 ± 0.0007	$1.82^{+0.25}_{-0.23}$	1
Kepler-1582 b	M5 V	0.217 ± 0.006	1.060 ± 0.071	$31.41^{+0.96}_{-0.94}$	$4.838177 \pm 8.8 \times 10^{-5}$	1.23 ± 0.04	0.0333 ± 0.0010	$3.75^{+0.50}_{-0.46}$	3

NOTE—References: (1) [Angelo et al. \(2017\)](#), (2) [Mann et al. \(2017\)](#), (3) [Morton et al. \(2016\)](#), (4) [Muirhead et al. \(2015\)](#)

Table 3. Stellar parameters for spectroscopically classified targets.

KIC ID	Distance (pc)	M_{K_S} (mag)	Telescope ^a	Spec. Type ^b	T_{eff}^c (K)	[Fe/H] (dex)	R_* (R_{\odot})	M_* (M_{\odot})
01995305	139.882 ± 1.253	6.784 ± 0.039	W/I	M3.5 V	3325	-0.426 ± 0.100	0.331 ± 0.010	0.320 ± 0.010
02164791	D/I	M4.5 Ve	3157	-0.166 ± 0.099	0.218 ± 0.044	0.182 ± 0.064
02283749	291.795 ± 6.182	5.546 ± 0.053	W	M4 Ve	3241	...	0.516 ± 0.017	0.518 ± 0.015
02693779	176.658 ± 1.632	6.308 ± 0.038	W	M4 V	3241	...	0.399 ± 0.013	0.394 ± 0.011
02832720	106.036 ± 5.989	6.352 ± 0.125	W/I	M4 Ve	3241	0.284 ± 0.152	0.398 ± 0.020	0.386 ± 0.022
02834637	125.012 ± 0.700	6.406 ± 0.023	W/I	M4 Ve	3241	0.063 ± 0.073	0.387 ± 0.011	0.378 ± 0.009
03219046	63.177 ± 0.308	8.621 ± 0.026	W	M5 Ve	3073	...	0.166 ± 0.005	0.134 ± 0.003
03232191	W	M4 V	3241	...	0.258 ± 0.053	0.226 ± 0.075
03330684	W	M7 V	2736	...	0.126 ± 0.018	0.091 ± 0.018
03340246	112.936 ± 0.784	7.414 ± 0.027	W	M4 V	3241	...	0.265 ± 0.008	0.236 ± 0.006
03453233	193.017 ± 4.811	7.819 ± 0.094	D	M4 V	3241	...	0.226 ± 0.011	0.194 ± 0.010
03561148	59.378 ± 0.128	6.319 ± 0.015	L	M4 V	3241	...	0.398 ± 0.012	0.392 ± 0.009
03629595	116.233 ± 0.590	7.001 ± 0.027	W/I	M4 V	3241	-0.070 ± 0.101	0.310 ± 0.009	0.289 ± 0.007
03631048	351.484 ± 4.550	4.449 ± 0.033	W/I	M4 Ve	3241	0.118 ± 0.059	0.286 ± 0.054	0.260 ± 0.082
03642851	200.723 ± 2.401	6.322 ± 0.038	W	M4 V	3241	...	0.398 ± 0.013	0.391 ± 0.011
03654827	94.367 ± 0.753	6.884 ± 0.027	W	M6 V	2904	...	0.325 ± 0.010	0.305 ± 0.008
03731321	86.438 ± 0.375	7.493 ± 0.022	I	M3.5 V	3325	0.044 ± 0.091	0.259 ± 0.007	0.227 ± 0.006
03940072	107.897 ± 5.365	5.541 ± 0.110	W/I	M5 V	3073	-0.066 ± 0.097	0.514 ± 0.023	0.519 ± 0.021
03941669	117.196 ± 0.621	6.969 ± 0.026	W/I	M4.5 V	3157	0.132 ± 0.075	0.317 ± 0.009	0.293 ± 0.008
03954332	150.850 ± 2.368	7.894 ± 0.065	D	M5 V	3073	...	0.220 ± 0.008	0.187 ± 0.007
04078409	76.338 ± 0.596	8.739 ± 0.037	D	M6 V	2904	...	0.158 ± 0.005	0.128 ± 0.003
04248433	36.985 ± 0.072	7.593 ± 0.018	W/I	M5.5 Ve	2989	0.296 ± 0.075	0.252 ± 0.007	0.216 ± 0.006
04270856	151.141 ± 2.118	6.432 ± 0.042	W	M2.5 V	3494	...	0.382 ± 0.012	0.374 ± 0.011
04448009	239.205 ± 4.375	6.246 ± 0.050	W	M4 V	3241	...	0.409 ± 0.014	0.404 ± 0.012
04470937	17.448 ± 0.033	6.131 ± 0.017	W	M2 V	3578	...	0.425 ± 0.013	0.423 ± 0.010
04545041	410.440 ± 23.898	4.064 ± 0.130	W/I	M3.5 Ve	3325	0.424 ± 0.110	0.357 ± 0.069	0.364 ± 0.108
04545209	175.733 ± 2.422	6.146 ± 0.039	W	M4 V	3241	...	0.423 ± 0.013	0.420 ± 0.011
04568065	82.102 ± 0.425	6.941 ± 0.023	W	M5 V	3073	...	0.318 ± 0.010	0.297 ± 0.007
04726552	157.506 ± 1.591	7.180 ± 0.039	W	M4 V	3241	...	0.290 ± 0.009	0.265 ± 0.008
04730040	227.179 ± 4.623	7.371 ± 0.068	D	M4 V	3241	...	0.270 ± 0.010	0.241 ± 0.010
04741907	119.957 ± 1.334	7.656 ± 0.037	W	M5 V	3073	...	0.241 ± 0.008	0.210 ± 0.006
04815654	64.279 ± 0.356	8.931 ± 0.030	D/W	M6 V	2904	...	0.148 ± 0.005	0.118 ± 0.003
04856658	119.571 ± 1.044	7.346 ± 0.032	W	M3 V	3410	...	0.272 ± 0.009	0.244 ± 0.007
04913121	66.698 ± 0.471	8.960 ± 0.038	D/W	M6 Ve	2904	...	0.146 ± 0.005	0.117 ± 0.003
04917182	91.451 ± 0.495	7.119 ± 0.023	W	M5.5 V	2989	...	0.297 ± 0.009	0.273 ± 0.007
04946433	117.314 ± 3.026	4.866 ± 0.060	W	M3.5 V	3325	...	0.636 ± 0.022	0.621 ± 0.017
05002836	28.142 ± 0.020	6.916 ± 0.017	W/I	M4 V	3241	-0.183 ± 0.086	0.319 ± 0.009	0.301 ± 0.007
05079348	76.937 ± 0.199	6.614 ± 0.020	W	M3.5 V	3325	...	0.358 ± 0.011	0.345 ± 0.008

Table 3 continued

Table 3 (continued)

KIC ID	Distance	M_{K_S}	Telescope ^a	Spec. Type ^b	T_{eff}^c	[Fe/H]	R_{\star}	M_{\star}
	(pc)	(mag)			(K)	(dex)	(R_{\odot})	(M_{\odot})
05122206	45.857 ± 0.080	6.689 ± 0.020	W	M4.5 V	3157	...	0.349 ± 0.010	0.334 ± 0.008
05126248	122.180 ± 1.109	6.441 ± 0.028	W	M5 V	3073	...	0.381 ± 0.012	0.372 ± 0.009
05175854	67.247 ± 0.371	8.789 ± 0.033	D/W	M7 Ve	2736	...	0.156 ± 0.005	0.125 ± 0.003
05181762	206.139 ± 2.134	5.703 ± 0.030	W	M4 V	3241	...	0.491 ± 0.015	0.493 ± 0.012
05256590	129.297 ± 1.581	8.145 ± 0.051	D	M5 V	3073	...	0.199 ± 0.007	0.166 ± 0.005
05304146	77.219 ± 0.772	6.464 ± 0.030	W	M6.5 Ve	2820	...	0.378 ± 0.012	0.369 ± 0.009
05341486	229.710 ± 23.293	5.717 ± 0.226	W	M5.5 Ve	2989	...	0.488 ± 0.038	0.489 ± 0.038
05353762	54.996 ± 0.374	9.361 ± 0.036	W	M7 V	2736	...	0.129 ± 0.004	0.102 ± 0.003
05354341	66.588 ± 0.183	7.420 ± 0.021	W	M4 Ve	3241	...	0.265 ± 0.008	0.236 ± 0.006
05438886	157.235 ± 1.454	6.946 ± 0.033	W	M4 V	3241	...	0.317 ± 0.010	0.296 ± 0.008
05513232	239.522 ± 3.730	5.296 ± 0.042	W	M4.5 Ve	3157	...	0.558 ± 0.018	0.557 ± 0.015
05513833	107.660 ± 1.513	6.412 ± 0.037	W	M4 V	3241	...	0.385 ± 0.012	0.377 ± 0.010
05515259	107.679 ± 0.724	7.660 ± 0.029	W	M3 Ve	3410	...	0.241 ± 0.007	0.209 ± 0.005
05602310	148.886 ± 2.970	5.862 ± 0.047	W/I	M4 V	3241	-0.054 ± 0.333	0.463 ± 0.014	0.467 ± 0.013
05603484	108.713 ± 0.447	6.629 ± 0.022	W	M4 V	3241	...	0.356 ± 0.011	0.343 ± 0.008
05603847	80.025 ± 0.487	8.491 ± 0.030	W	M5 V	3073	...	0.174 ± 0.005	0.142 ± 0.004
05649085	124.787 ± 0.831	6.833 ± 0.029	W	M3 Ve	3410	...	0.331 ± 0.010	0.313 ± 0.008
05791720	70.692 ± 0.185	6.185 ± 0.019	L	M3.5 Ve	3325	...	0.417 ± 0.012	0.414 ± 0.010
05818116	123.847 ± 0.573	6.428 ± 0.025	W	M2 V	3578	...	0.383 ± 0.012	0.374 ± 0.009
05859112	95.371 ± 0.430	7.075 ± 0.025	W/I	M4.5 V	3157	0.572 ± 0.101	0.310 ± 0.009	0.278 ± 0.008
05859124	154.233 ± 1.347	6.853 ± 0.033	W	M3.5 V	3325	...	0.328 ± 0.010	0.310 ± 0.008
05868793 ^d	78.891 ± 0.440	7.949 ± 0.026	W	M5 V	3073	0.120 ± 0.200	0.217 ± 0.006	0.182 ± 0.005
05868814	263.882 ± 5.816	6.214 ± 0.060	W	M3.5 V	3325	...	0.413 ± 0.015	0.409 ± 0.013
05943385	42.711 ± 0.089	7.360 ± 0.018	W/I	M4.5 V	3157	0.364 ± 0.172	0.276 ± 0.008	0.242 ± 0.006
05944764	159.531 ± 1.214	6.400 ± 0.027	W	M3.5 V	3325	...	0.387 ± 0.012	0.379 ± 0.009
05953947	111.177 ± 0.590	6.918 ± 0.025	W/I	M4 V	3241	-0.296 ± 0.112	0.317 ± 0.009	0.301 ± 0.008
06037009	133.160 ± 0.735	6.735 ± 0.027	W/I	M4 Ve	3241	-0.178 ± 0.140	0.340 ± 0.010	0.327 ± 0.009
06102091	136.951 ± 1.412	7.243 ± 0.042	W	M4 Ve	3241	...	0.283 ± 0.009	0.257 ± 0.008
06102845	125.299 ± 1.256	7.562 ± 0.045	W	M4 V	3241	...	0.251 ± 0.008	0.220 ± 0.007
06117602	20.941 ± 0.027	8.769 ± 0.018	I	M5 V	3073	-0.035 ± 0.075	0.157 ± 0.004	0.126 ± 0.003
06183400	74.079 ± 0.279	7.498 ± 0.023	W/I	M4 V	3241	-0.277 ± 0.098	0.254 ± 0.007	0.227 ± 0.006
06183736	140.704 ± 1.436	6.808 ± 0.040	W/I	M4 Ve	3241	0.180 ± 0.095	0.337 ± 0.010	0.316 ± 0.009
06187812	269.005 ± 3.559	5.038 ± 0.035	W/I	M3 Ve	3410	0.174 ± 0.195	0.607 ± 0.018	0.596 ± 0.016
06214037	218.767 ± 5.960	7.682 ± 0.103	D	M4 V	3241	...	0.239 ± 0.012	0.207 ± 0.011
06233711	57.618 ± 0.142	7.717 ± 0.022	D	M5 Ve	3073	...	0.236 ± 0.007	0.204 ± 0.005
06264426	150.494 ± 1.242	6.621 ± 0.037	W/I	M3 V	3410	-0.148 ± 0.067	0.355 ± 0.011	0.344 ± 0.010
06268411	95.286 ± 0.476	7.374 ± 0.023	W/I	M2.5 V	3494	-0.133 ± 0.105	0.269 ± 0.008	0.241 ± 0.006
06424725	154.652 ± 2.072	6.764 ± 0.038	W	M4 V	3241	...	0.339 ± 0.011	0.323 ± 0.009
06444896 ^e	92.191 ± 0.546	7.764 ± 0.029	W	M5 V	3073	-0.150 ± 0.110	0.231 ± 0.007	0.199 ± 0.005
06471285	D	M5 V	3073	...	0.190 ± 0.040	0.153 ± 0.052

Table 3 continued

Table 3 (continued)

KIC ID	Distance (pc)	M_{K_S} (mag)	Telescope ^a	Spec. Type ^b	T_{eff}^c (K)	[Fe/H] (dex)	R_* (R_\odot)	M_* (M_\odot)
06605595	85.366 ± 0.301	6.337 ± 0.018	W/I	M4 V	3241	0.291 ± 0.083	0.401 ± 0.011	0.389 ± 0.010
06665209	164.525 ± 3.590	8.293 ± 0.082	W	M5 V	3073	...	0.188 ± 0.008	0.155 ± 0.007
06672297	75.366 ± 0.294	7.468 ± 0.021	W	M4 V	3241	...	0.260 ± 0.008	0.230 ± 0.006
06676217	149.317 ± 1.230	7.113 ± 0.033	W	M4 V	3241	...	0.298 ± 0.009	0.274 ± 0.007
06693042	130.426 ± 1.071	5.818 ± 0.026	W/I	M4 V	3241	-0.299 ± 0.096	0.465 ± 0.013	0.474 ± 0.012
06752213	163.992 ± 1.565	7.100 ± 0.037	W	M4 V	3241	...	0.299 ± 0.010	0.275 ± 0.008
06761765	142.006 ± 1.282	7.162 ± 0.031	W	M4 V	3241	...	0.292 ± 0.009	0.267 ± 0.007
06768613	185.719 ± 3.521	7.525 ± 0.060	W	M4 V	3241	...	0.254 ± 0.009	0.224 ± 0.008
06776555	108.690 ± 0.481	7.053 ± 0.031	W/I	M4 V	3241	-0.117 ± 0.096	0.304 ± 0.009	0.282 ± 0.008
06783223	89.125 ± 0.913	8.602 ± 0.042	D	M7 Ve	2736	...	0.167 ± 0.006	0.135 ± 0.004
06784339	114.392 ± 1.100	8.140 ± 0.043	D/I	M6 V	2904	-0.074 ± 0.142	0.200 ± 0.006	0.166 ± 0.005
06805049	224.585 ± 3.035	6.025 ± 0.039	D	M4 V	3241	...	0.440 ± 0.014	0.440 ± 0.012
06837702	250.199 ± 17.033	5.324 ± 0.148	W	M4 Ve	3241	...	0.554 ± 0.030	0.552 ± 0.027
06847171	170.189 ± 1.015	5.795 ± 0.023	W/I	M4 V	3241	0.568 ± 0.087	0.487 ± 0.014	0.477 ± 0.013
07008143	47.933 ± 0.095	7.405 ± 0.012	W	M5 V	3073	...	0.266 ± 0.008	0.237 ± 0.005
07022137	114.244 ± 0.582	6.353 ± 0.019	W	M4 V	3241	...	0.393 ± 0.012	0.386 ± 0.009
07091150	124.185 ± 1.338	7.806 ± 0.038	W	M4.5 V	3157	...	0.227 ± 0.007	0.195 ± 0.006
07102366	200.921 ± 1.978	6.434 ± 0.035	W	M4 V	3241	...	0.382 ± 0.012	0.373 ± 0.010
07102500	152.605 ± 0.969	5.361 ± 0.022	W/I	M4 Ve	3241	0.185 ± 0.123	0.550 ± 0.015	0.547 ± 0.014
07177371	195.153 ± 2.322	6.110 ± 0.036	W/I	M5 V	3073	0.226 ± 0.071	0.432 ± 0.013	0.425 ± 0.012
07185487	245.782 ± 3.523	5.928 ± 0.039	W	M4 V	3241	...	0.455 ± 0.014	0.456 ± 0.012
07185789	110.923 ± 0.646	7.008 ± 0.023	W/I	M4 V	3241	0.011 ± 0.070	0.311 ± 0.009	0.288 ± 0.007
07272205	166.472 ± 1.413	6.157 ± 0.026	W	M3.5 V	3325	...	0.421 ± 0.013	0.418 ± 0.010
07304449 ^f	134.397 ± 0.721	6.555 ± 0.024	W	M3.5 V	3325	-0.110 ± 0.090	0.364 ± 0.010	0.355 ± 0.009
07341653	19.169 ± 0.017	7.509 ± 0.016	L	M5 Ve	3073	...	0.256 ± 0.008	0.226 ± 0.005
07350067 ^g	127.591 ± 0.617	6.498 ± 0.018	W	M4 Ve	3241	...	0.374 ± 0.011	0.363 ± 0.009
07352892	90.769 ± 0.461	7.235 ± 0.017	W	M4.5 V	3157	...	0.284 ± 0.008	0.258 ± 0.006
07500850	399.363 ± 12.883	4.935 ± 0.074	W	M4 Ve	3241	...	0.623 ± 0.023	0.611 ± 0.018
07505473	42.926 ± 0.759	7.737 ± 0.042	W/I	M5 Ve	3073	0.009 ± 0.095	0.235 ± 0.007	0.202 ± 0.006
07505644	293.822 ± 4.143	5.111 ± 0.039	W/I	M3 Ve	3410	0.179 ± 0.094	0.594 ± 0.018	0.585 ± 0.016
07517730	33.970 ± 0.078	8.889 ± 0.014	W	M6 V	2904	...	0.150 ± 0.004	0.120 ± 0.003
07582793	189.719 ± 2.246	7.172 ± 0.044	D/W	M3.5 V	3325	...	0.291 ± 0.010	0.266 ± 0.008
07596910	78.058 ± 0.347	5.968 ± 0.015	W	M4.5 V	3157	...	0.449 ± 0.013	0.449 ± 0.010
07659103	93.778 ± 0.371	6.971 ± 0.016	W/I	M4 V	3241	-0.266 ± 0.094	0.311 ± 0.009	0.293 ± 0.007
07661403	154.592 ± 1.384	6.472 ± 0.023	W	M4 Ve	3241	...	0.377 ± 0.011	0.367 ± 0.009
07729309	D/I	M2 V	3578	-0.204 ± 0.093	0.410 ± 0.060	0.405 ± 0.094
07734382	155.505 ± 2.173	7.255 ± 0.048	W	M4 Ve	3241	...	0.282 ± 0.010	0.255 ± 0.008
07799514	W	M4 V	3241	...	0.258 ± 0.053	0.226 ± 0.075
07799844	103.436 ± 1.095	8.559 ± 0.041	D	M6 V	2904	...	0.169 ± 0.006	0.138 ± 0.004
07809767	204.264 ± 6.670	7.960 ± 0.109	D	M5 V	3073	...	0.214 ± 0.011	0.181 ± 0.010

Table 3 continued

Table 3 (continued)

KIC ID	Distance	M_{K_S}	Telescope ^a	Spec. Type ^b	T_{eff}^c	[Fe/H]	R_*	M_*
	(pc)	(mag)			(K)	(dex)	(R_\odot)	(M_\odot)
07849191	57.455 ± 0.165	8.308 ± 0.023	W	M4 V	3241	...	0.187 ± 0.006	0.154 ± 0.004
07903237	439.487 ± 34.408	6.587 ± 0.173	D	M4 Ve	3241	...	0.362 ± 0.025	0.349 ± 0.028
07938787	154.623 ± 1.454	5.562 ± 0.023	W	M4 V	3241	...	0.513 ± 0.015	0.515 ± 0.012
07939565	65.472 ± 0.154	6.628 ± 0.012	W	M2.5 Ve	3494	...	0.357 ± 0.010	0.343 ± 0.008
08036551	93.164 ± 1.147	8.725 ± 0.047	D	M6 V	2904	...	0.159 ± 0.005	0.128 ± 0.004
08040522	253.639 ± 8.224	7.293 ± 0.097	D	M4 V	3241	...	0.278 ± 0.013	0.251 ± 0.013
08076831	48.598 ± 0.090	6.944 ± 0.012	W	M2.5 V	3494	...	0.317 ± 0.009	0.297 ± 0.007
08082302	157.362 ± 1.149	6.546 ± 0.029	W	M4 V	3241	...	0.367 ± 0.011	0.356 ± 0.009
08095972	114.779 ± 0.547	6.773 ± 0.020	W/I	M2 V	3578	-0.143 ± 0.093	0.336 ± 0.009	0.321 ± 0.008
08167877	323.982 ± 11.181	6.646 ± 0.112	W	M3 V	3410	...	0.354 ± 0.018	0.340 ± 0.019
08190958	47.983 ± 0.090	6.501 ± 0.020	W	M3.5 V	3325	...	0.373 ± 0.011	0.363 ± 0.009
08197652	W	M4 Ve	3241	...	0.258 ± 0.053	0.226 ± 0.075
08213019	220.989 ± 2.549	5.429 ± 0.029	W	M4 V	3241	...	0.536 ± 0.016	0.537 ± 0.013
08233951	102.901 ± 0.504	6.994 ± 0.025	W/I	M4 V	3241	-0.332 ± 0.097	0.307 ± 0.009	0.290 ± 0.008
08236114	140.875 ± 1.895	8.403 ± 0.082	D/W	M4 V	3241	...	0.180 ± 0.008	0.147 ± 0.006
08278279	183.522 ± 3.684	6.100 ± 0.047	W/I	M6 Ve	2904	0.530 ± 0.062	0.439 ± 0.014	0.427 ± 0.013
08284382	136.937 ± 1.112	7.118 ± 0.034	W	M3.5 V	3325	...	0.297 ± 0.009	0.273 ± 0.008
08302467	181.216 ± 1.335	5.938 ± 0.028	W	M4 Ve	3241	...	0.454 ± 0.014	0.454 ± 0.011
08331947	137.376 ± 1.105	7.199 ± 0.032	W	M4 V	3241	...	0.288 ± 0.009	0.262 ± 0.007
08332355	52.667 ± 0.134	7.398 ± 0.019	W	M5 Ve	3073	...	0.267 ± 0.008	0.238 ± 0.006
08344757	126.858 ± 0.928	7.617 ± 0.031	W	M4 V	3241	...	0.245 ± 0.008	0.214 ± 0.006
08387281	54.841 ± 0.123	6.469 ± 0.016	W/I	M3 Ve	3410	-0.026 ± 0.125	0.377 ± 0.010	0.368 ± 0.009
08416220	W	M4 Ve	3241	...	0.258 ± 0.053	0.226 ± 0.075
08423202	83.111 ± 0.762	8.728 ± 0.040	D	M6 Ve	2904	...	0.159 ± 0.005	0.128 ± 0.004
08428178	185.033 ± 7.618	6.056 ± 0.092	W/I	M2.5 V	3494	-0.163 ± 0.084	0.432 ± 0.018	0.435 ± 0.018
08431077	W	M4 V	3241	...	0.258 ± 0.053	0.226 ± 0.075
08451881	4.661 ± 0.002	9.044 ± 0.018	W/D	M7 Ve	2736	...	0.142 ± 0.004	0.113 ± 0.003
08452193	132.652 ± 0.861	6.709 ± 0.036	W/I	M2.5 V	3494	0.034 ± 0.086	0.347 ± 0.010	0.331 ± 0.009
08482923	72.997 ± 0.347	8.124 ± 0.023	W	M6.5 V	2820	...	0.201 ± 0.006	0.167 ± 0.004
08493421	44.741 ± 0.140	8.429 ± 0.017	I	M5 V	3073	0.358 ± 0.087	0.182 ± 0.005	0.145 ± 0.004
08496410	138.102 ± 0.893	6.759 ± 0.027	W	M4 V	3241	...	0.340 ± 0.010	0.323 ± 0.008
08507979	52.761 ± 0.096	6.207 ± 0.015	L	M3 Ve	3410	...	0.414 ± 0.012	0.410 ± 0.009
08548052	190.722 ± 2.081	6.551 ± 0.034	W	M4 V	3241	...	0.366 ± 0.011	0.355 ± 0.010
08556831	154.952 ± 1.290	5.644 ± 0.021	W/I	M2 V	3578	0.451 ± 0.066	0.509 ± 0.014	0.502 ± 0.013
08561063 ^h	40.060 ± 0.065	8.451 ± 0.018	W	M3 V	3410	-0.500 ± 0.090	0.174 ± 0.005	0.144 ± 0.004
08564198	69.174 ± 0.206	7.669 ± 0.017	W	M3 V	3410	...	0.240 ± 0.007	0.209 ± 0.005
08611599	153.221 ± 3.049	8.267 ± 0.073	D	M5 V	3073	...	0.190 ± 0.008	0.157 ± 0.006
08611876	103.041 ± 0.390	6.459 ± 0.015	W	M4 Ve	3241	...	0.379 ± 0.011	0.369 ± 0.009
08647238	146.637 ± 1.020	6.332 ± 0.032	W	M4 V	3241	...	0.396 ± 0.012	0.390 ± 0.010
08655334	111.451 ± 0.603	6.572 ± 0.022	W	M4 V	3241	...	0.364 ± 0.011	0.352 ± 0.009

Table 3 continued

Table 3 (continued)

KIC ID	Distance (pc)	M_{K_S} (mag)	Telescope ^a	Spec. Type ^b	T_{eff}^c (K)	[Fe/H] (dex)	R_* (R_{\odot})	M_* (M_{\odot})
08669203	189.824 ± 2.944	6.528 ± 0.041	W	M4 V	3241	...	0.370 ± 0.012	0.358 ± 0.010
08733898 ⁱ	96.339 ± 0.511	7.908 ± 0.026	W	M4 V	3241	-0.300 ± 0.110	0.217 ± 0.006	0.186 ± 0.005
08776305	78.547 ± 0.271	6.925 ± 0.031	W/I	M5 V	3073	-0.337 ± 0.123	0.315 ± 0.009	0.300 ± 0.008
08804334	157.213 ± 2.042	7.150 ± 0.044	W	M5 Ve	3073	...	0.294 ± 0.010	0.269 ± 0.008
08815854	190.458 ± 4.039	7.482 ± 0.066	D	M4 V	3241	...	0.258 ± 0.010	0.229 ± 0.009
08837812	158.900 ± 1.929	7.139 ± 0.039	W	M4.5 V	3157	...	0.295 ± 0.010	0.270 ± 0.008
08869922	51.289 ± 0.145	7.475 ± 0.019	I	M4.5 V	3157	0.165 ± 0.113	0.262 ± 0.007	0.229 ± 0.006
08872565	20.539 ± 0.030	7.464 ± 0.014	W	M4 V	3241	...	0.260 ± 0.008	0.231 ± 0.005
0888543	71.042 ± 0.362	5.821 ± 0.022	W/I/L	M2 V	3578	0.244 ± 0.117	0.476 ± 0.013	0.473 ± 0.012
08933586	W	M5 V	3073	...	0.190 ± 0.040	0.153 ± 0.052
08937178	W	M4 V	3241	...	0.258 ± 0.053	0.226 ± 0.075
08939955	199.789 ± 1.981	6.324 ± 0.034	W	M4 V	3241	...	0.397 ± 0.012	0.391 ± 0.010
08956025	140.728 ± 1.180	6.504 ± 0.031	W	M4 Ve	3241	...	0.373 ± 0.012	0.362 ± 0.009
08977910	112.293 ± 0.557	6.267 ± 0.025	W/I	M4 Ve	3241	-0.011 ± 0.099	0.405 ± 0.011	0.400 ± 0.010
09004724	105.523 ± 0.670	7.943 ± 0.033	W	M5 V	3073	...	0.215 ± 0.007	0.182 ± 0.005
09005690	106.161 ± 1.116	8.475 ± 0.055	W	M5 Ve	3073	...	0.175 ± 0.006	0.143 ± 0.005
09113974	132.711 ± 1.236	6.751 ± 0.028	W	M3 Ve	3410	...	0.341 ± 0.010	0.324 ± 0.008
09117378	115.224 ± 1.127	8.184 ± 0.055	L	M3 V	3410	...	0.196 ± 0.007	0.163 ± 0.006
09138406	227.707 ± 3.460	6.241 ± 0.046	W	M3 Ve	3410	...	0.409 ± 0.014	0.404 ± 0.012
09138452	W/I	M3 V	3410	-0.201 ± 0.119	0.328 ± 0.057	0.305 ± 0.088
09202152	155.004 ± 1.659	6.995 ± 0.040	W	M2 V	3578	...	0.311 ± 0.010	0.290 ± 0.008
09202551	212.437 ± 2.933	6.354 ± 0.044	W	M3 V	3410	...	0.393 ± 0.013	0.386 ± 0.011
09203794	52.402 ± 0.095	6.464 ± 0.016	D/L/I	M4 V	3241	0.037 ± 0.067	0.379 ± 0.010	0.369 ± 0.009
09222296	91.386 ± 0.334	6.661 ± 0.018	W	M4.5 V	3157	...	0.352 ± 0.010	0.338 ± 0.008
09265282	114.141 ± 0.814	7.399 ± 0.031	W	M4 V	3241	...	0.267 ± 0.008	0.238 ± 0.006
09328653	180.700 ± 2.079	6.692 ± 0.042	W	M3 Ve	3410	...	0.348 ± 0.011	0.333 ± 0.010
09346063	105.363 ± 0.427	6.941 ± 0.029	W/I	M2 V	3578	-0.163 ± 0.085	0.316 ± 0.009	0.297 ± 0.008
09426508	92.564 ± 0.356	6.941 ± 0.025	W	M4.5 V	3157	...	0.318 ± 0.010	0.297 ± 0.007
09446620	358.768 ± 8.843	5.522 ± 0.066	D/W	M2.5 V	3494	...	0.520 ± 0.018	0.522 ± 0.016
09508489	78.168 ± 0.286	6.964 ± 0.014	W	M3 V	3410	...	0.315 ± 0.009	0.294 ± 0.007
09508904	188.176 ± 2.188	7.022 ± 0.042	W	M2 V	3578	...	0.308 ± 0.010	0.286 ± 0.009
09530511	167.032 ± 1.332	5.915 ± 0.026	W/I	M3 V	3410	-0.099 ± 0.075	0.455 ± 0.013	0.458 ± 0.011
09531271	294.556 ± 6.679	6.096 ± 0.064	W	M3.5 V	3325	...	0.430 ± 0.016	0.428 ± 0.014
09532950	336.753 ± 8.495	5.330 ± 0.063	W	M6 Ve	2904	...	0.552 ± 0.019	0.552 ± 0.016
09533618	848.292 ± 157.725	5.598 ± 0.453	W	M2 V	3578	...	0.506 ± 0.073	0.510 ± 0.073
09582827	147.322 ± 1.323	6.338 ± 0.025	W/I/L	M4 V	3241	-0.329 ± 0.122	0.390 ± 0.011	0.389 ± 0.010
09591560	224.479 ± 1.982	4.824 ± 0.031	W	M3.5 Ve	3325	...	0.644 ± 0.020	0.627 ± 0.016
09593432	359.228 ± 46.191	5.463 ± 0.291	W	M3 Ve	3410	...	0.531 ± 0.050	0.532 ± 0.047
09595546	178.491 ± 38.506	8.698 ± 0.511	W	M4 Ve	3241	...	0.160 ± 0.029	0.129 ± 0.026
09605714	250.049 ± 11.127	5.205 ± 0.100	W	M2 V	3578	...	0.574 ± 0.024	0.571 ± 0.020

Table 3 continued

Table 3 (continued)

KIC ID	Distance	M_{K_S}	Telescope ^a	Spec. Type ^b	T_{eff}^c	[Fe/H]	R_*	M_*
	(pc)	(mag)			(K)	(dex)	(R_\odot)	(M_\odot)
09605900	255.863 ± 3.131	4.997 ± 0.034	W	M2.5 V	3494	...	0.612 ± 0.019	0.602 ± 0.015
09611538	154.040 ± 1.457	6.512 ± 0.027	W	M4 V	3241	...	0.372 ± 0.011	0.361 ± 0.009
09612825	92.749 ± 0.443	7.296 ± 0.028	W	M4 V	3241	...	0.278 ± 0.009	0.250 ± 0.007
09642890	123.742 ± 1.108	6.388 ± 0.026	W/I	M4 V	3241	0.245 ± 0.077	0.393 ± 0.011	0.380 ± 0.010
09643210	105.653 ± 0.498	6.894 ± 0.021	W/I	M3 Ve	3410	-0.135 ± 0.067	0.322 ± 0.009	0.304 ± 0.008
09654450	194.946 ± 2.913	5.579 ± 0.039	W/I	M3 V	3410	0.098 ± 0.104	0.512 ± 0.015	0.513 ± 0.014
09654642	118.885 ± 0.959	7.457 ± 0.030	W	M5 V	3073	...	0.261 ± 0.008	0.231 ± 0.006
09654803	D	M2 Ve	3578	...	0.428 ± 0.074	0.427 ± 0.109
09655532	227.689 ± 10.071	7.749 ± 0.130	W	M4.5 V	3157	...	0.233 ± 0.014	0.200 ± 0.014
09655679	504.443 ± 61.359	6.668 ± 0.320	D/W	M4 V	3241	...	0.352 ± 0.042	0.338 ± 0.048
09705079	117.070 ± 0.977	6.279 ± 0.021	W/I/L	M4.5 V	3157	-0.078 ± 0.126	0.402 ± 0.011	0.398 ± 0.010
09715286	349.410 ± 26.335	7.452 ± 0.237	D	M4 V	3241	...	0.262 ± 0.025	0.232 ± 0.027
09715460	164.873 ± 1.773	6.461 ± 0.034	W	M4 V	3241	...	0.379 ± 0.012	0.369 ± 0.010
09715957	428.860 ± 22.777	6.763 ± 0.174	W	M3.5 V	3325	...	0.340 ± 0.024	0.323 ± 0.027
09715985	288.748 ± 12.699	7.147 ± 0.131	W	M5 V	3073	...	0.294 ± 0.017	0.269 ± 0.018
09716727	651.018 ± 80.781	5.954 ± 0.313	W	M3.5 V	3325	...	0.452 ± 0.049	0.453 ± 0.052
09717123	644.470 ± 83.958	4.975 ± 0.295	W	M4 V	3241	...	0.616 ± 0.057	0.605 ± 0.046
09717341	385.669 ± 11.992	6.055 ± 0.089	D/W	M3.5 V	3325	...	0.436 ± 0.018	0.435 ± 0.018
09726699	11.975 ± 0.005	7.381 ± 0.016	W/L	M4.5 Ve	3157	...	0.269 ± 0.008	0.240 ± 0.006
09730163 ^j	127.201 ± 0.995	7.084 ± 0.033	W/L	M4.5 V	3157	0.270 ± 0.090	0.305 ± 0.009	0.277 ± 0.008
09776037	260.188 ± 7.487	6.353 ± 0.074	D/W	M5 Ve	3073	...	0.393 ± 0.015	0.386 ± 0.014
09776485	388.865 ± 20.188	6.492 ± 0.143	W	M4.5 V	3157	...	0.374 ± 0.022	0.364 ± 0.024
09825426	138.628 ± 1.660	5.758 ± 0.029	W/I	M3 V	3410	-0.212 ± 0.114	0.476 ± 0.014	0.484 ± 0.012
09836326	631.240 ± 79.199	6.300 ± 0.280	D/W	M4 V	3241	...	0.400 ± 0.041	0.395 ± 0.045
09836425	261.507 ± 4.515	6.206 ± 0.052	W	M4 V	3241	...	0.414 ± 0.014	0.410 ± 0.012
09836628	589.574 ± 42.705	5.360 ± 0.173	D/W	M4 Ve	3241	...	0.548 ± 0.034	0.547 ± 0.030
09836691	129.458 ± 5.277	7.395 ± 0.093	W	M7 Ve	2736	...	0.267 ± 0.012	0.239 ± 0.012
09836833	699.840 ± 82.937	5.650 ± 0.289	D	M4 Ve	3241	...	0.499 ± 0.049	0.501 ± 0.048
09836960	407.031 ± 31.267	6.493 ± 0.194	W	M4.5 Ve	3157	...	0.375 ± 0.028	0.364 ± 0.031
09838000	192.179 ± 2.047	6.485 ± 0.035	W	M3.5 V	3325	...	0.375 ± 0.012	0.365 ± 0.010
09838371	418.407 ± 29.991	6.460 ± 0.182	W	M4 V	3241	...	0.378 ± 0.027	0.369 ± 0.030
09880519	288.954 ± 5.492	5.343 ± 0.048	W	M5 Ve	3073	...	0.551 ± 0.018	0.550 ± 0.015
09897336	775.511 ± 131.215	5.153 ± 0.396	W	M4 V	3241	...	0.582 ± 0.070	0.577 ± 0.062
09897967	187.414 ± 2.125	6.008 ± 0.035	W	M4.5 V	3157	...	0.443 ± 0.014	0.443 ± 0.012
09953754	127.563 ± 0.721	6.334 ± 0.023	W	M3 V	3410	...	0.396 ± 0.012	0.389 ± 0.009
09957818	251.354 ± 7.707	6.418 ± 0.078	W	M4 V	3241	...	0.384 ± 0.015	0.376 ± 0.015
09992786	69.626 ± 0.244	7.604 ± 0.022	W	M5 V	3073	...	0.246 ± 0.007	0.215 ± 0.005
10017286	W	M4 V	3241	...	0.258 ± 0.053	0.226 ± 0.075
10024566	162.190 ± 1.261	6.502 ± 0.028	W	M2.5 V	3494	...	0.373 ± 0.011	0.363 ± 0.009
10063466	W/I	M2 V	3578	-0.361 ± 0.073	0.379 ± 0.054	0.366 ± 0.084

Table 3 continued

Table 3 (continued)

KIC ID	Distance (pc)	M_{K_S} (mag)	Telescope ^a	Spec. Type ^b	T_{eff}^c (K)	[Fe/H] (dex)	R_* (R_\odot)	M_* (M_\odot)
10066002	104.355 ± 1.565	6.732 ± 0.035	W	M4 V	3241	...	0.343 ± 0.011	0.327 ± 0.009
10069097	86.155 ± 0.275	6.786 ± 0.018	I	M2.5 V	3494	-0.603 ± 0.116	0.328 ± 0.009	0.320 ± 0.009
10193199	57.142 ± 0.090	5.842 ± 0.015	W	M3 V	3410	...	0.469 ± 0.014	0.470 ± 0.011
10251759	405.980 ± 130.481	4.793 ± 0.847	D/W	M4 V	3241	...	0.648 ± 0.137	0.631 ± 0.126
10258179	26.658 ± 0.084	6.475 ± 0.017	L	M2.5 V	3494	...	0.377 ± 0.011	0.367 ± 0.009
10275253	213.549 ± 2.694	6.073 ± 0.039	W	M5 V	3073	...	0.433 ± 0.014	0.432 ± 0.012
10285569	35.329 ± 0.061	8.261 ± 0.015	W	M5 Ve	3073	...	0.190 ± 0.006	0.157 ± 0.004
10318386	193.184 ± 2.005	6.250 ± 0.030	W	M4 Ve	3241	...	0.408 ± 0.013	0.403 ± 0.010
10324321	139.247 ± 1.106	6.695 ± 0.031	W	M4 V	3241	...	0.348 ± 0.011	0.333 ± 0.009
10330511	100.701 ± 0.534	7.471 ± 0.023	W	M4 V	3241	...	0.259 ± 0.008	0.230 ± 0.006
10339336	221.044 ± 3.362	6.616 ± 0.052	W	M2 V	3578	...	0.358 ± 0.012	0.345 ± 0.011
10351279	113.057 ± 0.790	7.801 ± 0.029	W	M5 V	3073	...	0.228 ± 0.007	0.195 ± 0.005
10384327	290.039 ± 4.988	5.507 ± 0.045	W	M3.5 V	3325	...	0.522 ± 0.017	0.524 ± 0.014
10396501	76.959 ± 0.220	6.748 ± 0.014	W	M4 V	3241	...	0.341 ± 0.010	0.325 ± 0.008
10448377	230.593 ± 3.718	5.117 ± 0.039	W/I	M5 Ve	3073	-0.105 ± 0.081	0.585 ± 0.017	0.585 ± 0.015
10449173	198.284 ± 2.250	6.808 ± 0.039	W	M4 V	3241	...	0.334 ± 0.011	0.316 ± 0.009
10452252	101.197 ± 0.477	6.068 ± 0.020	W	M5 Ve	3073	...	0.434 ± 0.013	0.433 ± 0.010
10455009	123.820 ± 0.685	6.465 ± 0.025	W	M4 V	3241	...	0.378 ± 0.011	0.368 ± 0.009
10459524	142.149 ± 0.870	6.959 ± 0.027	W	M2 V	3578	...	0.316 ± 0.010	0.295 ± 0.008
10471434	108.065 ± 1.421	8.539 ± 0.059	D/W	M6.5 Ve	2820	...	0.171 ± 0.006	0.139 ± 0.005
10538002	W	M5 Ve	3073	...	0.190 ± 0.040	0.153 ± 0.052
10548640	145.942 ± 1.037	6.067 ± 0.024	W/I	M4 Ve	3241	0.138 ± 0.070	0.437 ± 0.012	0.433 ± 0.011
10548992	218.466 ± 8.134	7.562 ± 0.110	D	M5 V	3073	...	0.251 ± 0.013	0.220 ± 0.013
10585782	172.808 ± 1.263	6.215 ± 0.029	W	M3.5 V	3325	...	0.413 ± 0.013	0.409 ± 0.010
10599274	W/I	M4 V	3241	0.084 ± 0.107	0.282 ± 0.055	0.252 ± 0.085
10647081	19.622 ± 0.011	6.436 ± 0.016	L	M4 V	3241	...	0.382 ± 0.011	0.373 ± 0.009
10647233	362.733 ± 7.383	5.503 ± 0.062	W	M4 V	3241	...	0.523 ± 0.018	0.524 ± 0.016
10647424	135.812 ± 1.543	7.695 ± 0.048	D/W	M5 Ve	3073	...	0.238 ± 0.008	0.206 ± 0.007
10665619	W/I	M5 V	3073	0.202 ± 0.095	0.212 ± 0.043	0.176 ± 0.062
10668092	243.884 ± 3.487	6.321 ± 0.053	W	M3 V	3410	...	0.398 ± 0.014	0.391 ± 0.012
10709619	99.795 ± 0.380	6.532 ± 0.019	W	M4 V	3241	...	0.369 ± 0.011	0.358 ± 0.008
10710233	W	M4 Ve	3241	...	0.258 ± 0.053	0.226 ± 0.075
10711003	127.830 ± 2.921	8.460 ± 0.086	W	M7 Ve	2736	...	0.176 ± 0.008	0.144 ± 0.006
10731839	26.153 ± 0.171	6.254 ± 0.023	W/L	M4.5 V	3157	...	0.407 ± 0.012	0.402 ± 0.010
10732063	154.612 ± 0.829	5.887 ± 0.023	W/I	M4 V	3241	0.071 ± 0.088	0.462 ± 0.013	0.463 ± 0.011
10777226	96.893 ± 1.496	8.718 ± 0.060	W	M7 V	2736	...	0.160 ± 0.006	0.129 ± 0.004
10841791	126.918 ± 2.124	8.207 ± 0.067	D/W	M5 Ve	3073	...	0.194 ± 0.008	0.161 ± 0.006
10843766	262.771 ± 3.264	5.895 ± 0.041	W	M2.5 V	3494	...	0.460 ± 0.015	0.461 ± 0.012
10860741	30.758 ± 0.038	8.156 ± 0.014	W	M6 V	2904	...	0.198 ± 0.006	0.165 ± 0.004
10910277	217.363 ± 4.779	6.744 ± 0.063	D	M5 V	3073	...	0.342 ± 0.013	0.325 ± 0.012

Table 3 continued

Table 3 (continued)

KIC ID	Distance	M_{K_S}	Telescope ^a	Spec. Type ^b	T_{eff}^c	[Fe/H]	R_*	M_*
	(pc)	(mag)			(K)	(dex)	(R_\odot)	(M_\odot)
10960093	123.132 ± 0.529	6.430 ± 0.020	W	M3.5 V	3325	...	0.383 ± 0.011	0.374 ± 0.009
11013311	196.892 ± 6.684	8.954 ± 0.082	D	M5 V	3073	...	0.146 ± 0.006	0.117 ± 0.004
11137723	112.801 ± 0.445	6.281 ± 0.021	W	M4 Ve	3241	...	0.403 ± 0.012	0.398 ± 0.010
11137924	101.202 ± 2.217	6.449 ± 0.051	W	M4 V	3241	...	0.380 ± 0.013	0.371 ± 0.011
11145819	149.751 ± 0.892	4.989 ± 0.021	W/I	M5 Ve	3073	0.222 ± 0.134	0.617 ± 0.017	0.603 ± 0.016
11187320	174.185 ± 3.601	7.995 ± 0.075	D	M3.5 V	3325	...	0.211 ± 0.009	0.178 ± 0.007
11288756	60.081 ± 0.192	7.587 ± 0.023	I	M5 V	3073	0.002 ± 0.068	0.249 ± 0.007	0.217 ± 0.005
11341162	152.577 ± 0.895	6.092 ± 0.028	I	M3.5 V	3325	0.065 ± 0.069	0.431 ± 0.012	0.429 ± 0.011
11356952	61.885 ± 0.556	8.639 ± 0.033	D	M7 Ve	2736	...	0.164 ± 0.005	0.133 ± 0.003
11462594	106.546 ± 0.421	6.728 ± 0.020	W	M4 V	3241	...	0.344 ± 0.010	0.328 ± 0.008
11462900	112.366 ± 0.447	6.431 ± 0.019	W/I	M4 V	3241	-0.149 ± 0.078	0.380 ± 0.011	0.374 ± 0.009
11551165	151.267 ± 1.286	7.001 ± 0.038	W	M1.5 V	3662	...	0.310 ± 0.010	0.289 ± 0.008
11602561	82.303 ± 0.354	7.670 ± 0.028	W/I	M6.5 V	2820	0.149 ± 0.078	0.243 ± 0.007	0.208 ± 0.006
11603184	244.989 ± 3.436	6.356 ± 0.046	W	M4 V	3241	...	0.393 ± 0.013	0.386 ± 0.011
11654343	222.610 ± 2.307	5.859 ± 0.036	W	M3.5 V	3325	...	0.466 ± 0.015	0.467 ± 0.012
11702373	177.349 ± 3.446	7.909 ± 0.085	D/W	M4 V	3241	...	0.218 ± 0.010	0.185 ± 0.009
11709473	203.356 ± 2.966	5.974 ± 0.039	W	M4 V	3241	...	0.448 ± 0.014	0.448 ± 0.012
11709752	46.157 ± 0.202	8.513 ± 0.026	I	M6.5 V	2820	0.015 ± 0.163	0.174 ± 0.005	0.140 ± 0.004
11710163	226.710 ± 3.479	5.986 ± 0.044	W	M6 Ve	2904	...	0.446 ± 0.015	0.446 ± 0.012
11717068	187.740 ± 4.127	7.638 ± 0.082	W	M4.5 V	3157	...	0.243 ± 0.010	0.212 ± 0.010
11717289	119.830 ± 2.110	8.570 ± 0.076	W	M7 V	2736	...	0.169 ± 0.007	0.137 ± 0.005
11724582	64.260 ± 0.302	7.907 ± 0.023	W	M6 V	2904	...	0.219 ± 0.007	0.186 ± 0.005
11751991	148.861 ± 1.136	6.003 ± 0.030	W	M2.5 V	3494	...	0.444 ± 0.014	0.443 ± 0.011
11752690	96.867 ± 0.587	7.431 ± 0.027	W	M4.5 Ve	3157	...	0.263 ± 0.008	0.234 ± 0.006
11769369	257.784 ± 3.631	5.223 ± 0.038	W	M4 V	3241	...	0.571 ± 0.018	0.569 ± 0.015
11810611	126.222 ± 0.654	6.928 ± 0.026	W	M2 V	3578	...	0.319 ± 0.010	0.299 ± 0.008
11861787	74.669 ± 0.221	7.212 ± 0.028	I	M4.5 V	3157	-0.051 ± 0.079	0.287 ± 0.008	0.261 ± 0.007
11868209	46.035 ± 0.086	7.680 ± 0.019	W	M4.5 V	3157	...	0.239 ± 0.007	0.207 ± 0.005
11876227	157.399 ± 1.130	6.036 ± 0.028	W	M4 Ve	3241	...	0.439 ± 0.013	0.438 ± 0.011
11918550	18.331 ± 0.020	6.832 ± 0.016	L	M3 V	3410	...	0.331 ± 0.010	0.313 ± 0.007
11920155	224.137 ± 2.734	5.829 ± 0.038	W	M4 V	3241	...	0.471 ± 0.015	0.472 ± 0.012
11925804	49.055 ± 0.086	6.935 ± 0.015	W	M4 Ve	3241	...	0.318 ± 0.009	0.298 ± 0.007
11957647	175.160 ± 1.275	6.012 ± 0.027	W/I	M2.5 Ve	3494	0.065 ± 0.127	0.443 ± 0.013	0.442 ± 0.011
12059261	151.438 ± 0.984	6.100 ± 0.028	W/I	M4 V	3241	0.107 ± 0.081	0.431 ± 0.012	0.427 ± 0.011
12066676	122.267 ± 0.803	6.761 ± 0.028	W/I	M4 V	3241	0.107 ± 0.114	0.342 ± 0.010	0.323 ± 0.008
12068325	71.119 ± 0.282	8.501 ± 0.029	W	M5 V	3073	...	0.173 ± 0.005	0.141 ± 0.004
12108566	79.661 ± 0.439	7.831 ± 0.027	W/I	M6 Ve	2904	0.131 ± 0.106	0.228 ± 0.007	0.192 ± 0.005
12159633	107.774 ± 0.472	6.140 ± 0.019	D/I	M4 V	3241	0.276 ± 0.080	0.428 ± 0.012	0.421 ± 0.010
12166644	105.885 ± 0.339	6.235 ± 0.018	W	M4 V	3241	...	0.410 ± 0.012	0.405 ± 0.009
12204358	171.869 ± 1.549	6.501 ± 0.030	W	M4 V	3241	...	0.373 ± 0.012	0.363 ± 0.009

Table 3 continued

Table 3 (*continued*)

KIC ID	Distance	M_{K_S}	Telescope ^a	Spec. Type ^b	T_{eff}^c	[Fe/H]	R_*	M_*
	(pc)	(mag)			(K)	(dex)	(R_\odot)	(M_\odot)
12302994	161.881 ± 1.346	6.137 ± 0.028	W/I	M4.5 V	3157	-0.068 ± 0.137	0.422 ± 0.012	0.421 ± 0.011
12306639	209.393 ± 6.284	7.839 ± 0.108	D	M6 V	2904	...	0.224 ± 0.012	0.192 ± 0.011
12351607	187.389 ± 1.884	6.315 ± 0.039	W	M4 V	3241	...	0.399 ± 0.013	0.392 ± 0.011
12505701	166.641 ± 1.431	5.930 ± 0.030	W/I	M5 V	3073	0.606 ± 0.070	0.467 ± 0.013	0.455 ± 0.013
12506640	97.789 ± 0.393	6.634 ± 0.025	W/I	M2 V	3578	-0.313 ± 0.066	0.351 ± 0.010	0.342 ± 0.009
12644136	43.998 ± 0.080	7.640 ± 0.020	I	M4.5 V	3157	0.141 ± 0.067	0.245 ± 0.007	0.211 ± 0.005
12688403	110.782 ± 0.765	6.242 ± 0.030	W/I	M3 Ve	3410	-0.194 ± 0.079	0.405 ± 0.012	0.404 ± 0.011
12689068	170.244 ± 1.519	6.650 ± 0.032	W	M2.5 V	3494	...	0.354 ± 0.011	0.340 ± 0.009
12735296	248.393 ± 35.087	5.459 ± 0.318	W	M2.5 V	3494	...	0.531 ± 0.054	0.532 ± 0.052

^aD = DCT, I = IRTF, L = LAMOST, W = WIYN

^bStars that exhibit H α emission from a by-eye analysis are classified with the peculiar flag ‘e’ to denote emission.

^cWe adopt a ± 88 K uncertainty for all temperatures from our spectral type vs. T_{eff} fit (Section 3.3).

^dKepler-1582

^eKepler-1649

^fKepler-1650

^gKepler-1646

^hKepler-42

ⁱKepler-446

^jKepler-445

Table 4. Stellar parameters for photometrically classified targets.

KIC ID	Distance	M_{K_S}	Spec. Type	T_{eff}^a	R_*	M_*
	(pc)	(mag)		(K)	(R_\odot)	(M_\odot)
01433760	192.959 ± 2.769	6.697 ± 0.046	M3 V	3410	0.348 ± 0.012	0.333 ± 0.010
02831828	106.525 ± 1.537	8.923 ± 0.056	M5 V	3073	0.148 ± 0.005	0.119 ± 0.004
02971472	40.706 ± 0.059	6.979 ± 0.019	M5 V	3073	0.313 ± 0.009	0.292 ± 0.007
02983661	148.672 ± 1.211	6.832 ± 0.029	M3 V	3410	0.331 ± 0.010	0.313 ± 0.008
03101838	201.853 ± 2.262	5.846 ± 0.032	M3 V	3410	0.468 ± 0.014	0.469 ± 0.012
03228276	111.970 ± 0.562	6.865 ± 0.025	M3 V	3410	0.327 ± 0.010	0.308 ± 0.008
03443923	144.103 ± 0.963	5.575 ± 0.026	M4 V	3241	0.511 ± 0.015	0.513 ± 0.013
03545104	45.524 ± 0.073	7.464 ± 0.019	M5 V	3073	0.260 ± 0.008	0.231 ± 0.006
03556888	172.661 ± 1.983	6.683 ± 0.042	M4 V	3241	0.349 ± 0.011	0.335 ± 0.010
03629762	23.997 ± 0.023	6.578 ± 0.017	M4 V	3241	0.363 ± 0.011	0.351 ± 0.008
03735000	110.168 ± 0.877	7.226 ± 0.030	M5 V	3073	0.285 ± 0.009	0.259 ± 0.007

Table 4 continued

Table 4 (*continued*)

KIC ID	Distance	M_{K_S}	Spec. Type	T_{eff}^a	R_*	M_*
	(pc)	(mag)		(K)	(R_{\odot})	(M_{\odot})
03838516	178.840 ± 2.708	7.298 ± 0.052	M4 V	3241	0.277 ± 0.010	0.250 ± 0.008
04037286	202.408 ± 3.214	6.687 ± 0.048	M4 V	3241	0.349 ± 0.012	0.334 ± 0.010
04039602	139.252 ± 1.341	7.816 ± 0.040	M4 V	3241	0.227 ± 0.007	0.194 ± 0.006
04068926	163.753 ± 2.285	7.340 ± 0.054	M5 V	3073	0.273 ± 0.010	0.245 ± 0.008
04137629	83.718 ± 0.346	7.454 ± 0.026	M4 V	3241	0.261 ± 0.008	0.232 ± 0.006
04142913	27.730 ± 0.093	4.948 ± 0.023	M4 V	3241	0.621 ± 0.018	0.609 ± 0.015
04173772	45.276 ± 0.066	6.568 ± 0.018	M4 V	3241	0.364 ± 0.011	0.352 ± 0.008
04466520	100.476 ± 0.332	5.642 ± 0.021	M2 V	3578	0.500 ± 0.015	0.503 ± 0.012
04581084	41.656 ± 0.077	6.385 ± 0.015	M5 V	3073	0.389 ± 0.011	0.381 ± 0.009
04644194	92.933 ± 0.480	7.493 ± 0.028	M4 V	3241	0.257 ± 0.008	0.227 ± 0.006
04862505	194.457 ± 2.170	5.798 ± 0.033	M4 V	3241	0.475 ± 0.015	0.477 ± 0.012
04909186	111.369 ± 0.366	5.665 ± 0.021	M3 V	3410	0.497 ± 0.015	0.499 ± 0.012
04921143	152.266 ± 3.613	5.281 ± 0.055	M3 V	3410	0.561 ± 0.019	0.560 ± 0.016
04938090	53.110 ± 0.185	7.916 ± 0.018	M5 V	3073	0.218 ± 0.006	0.185 ± 0.004
04997179	157.380 ± 1.758	5.677 ± 0.033	M2 V	3578	0.495 ± 0.015	0.497 ± 0.013
05112508	154.262 ± 0.864	5.767 ± 0.024	M3 V	3410	0.480 ± 0.014	0.482 ± 0.012
05256612	66.222 ± 0.241	8.122 ± 0.028	M4 V	3241	0.201 ± 0.006	0.168 ± 0.004
05435955	148.841 ± 3.469	6.083 ± 0.055	M4 V	3241	0.432 ± 0.015	0.430 ± 0.013
05435958	474.253 ± 13.718	4.958 ± 0.072	M3 V	3410	0.619 ± 0.022	0.608 ± 0.018
05522356	134.862 ± 4.891	8.752 ± 0.116	M6 V	2904	0.158 ± 0.008	0.127 ± 0.007
05597723	113.820 ± 0.971	7.749 ± 0.040	M5 V	3073	0.233 ± 0.008	0.200 ± 0.006
05608002	193.248 ± 11.800	5.710 ± 0.136	M4 V	3241	0.489 ± 0.026	0.491 ± 0.025
05630476	98.355 ± 0.637	7.433 ± 0.030	M4 V	3241	0.263 ± 0.008	0.234 ± 0.006
05716508	M3 V	3410	0.341 ± 0.064	0.321 ± 0.093
05802041	109.550 ± 0.667	7.198 ± 0.026	M4 V	3241	0.288 ± 0.009	0.263 ± 0.007
05855479	91.617 ± 0.936	8.983 ± 0.062	M5 V	3073	0.145 ± 0.005	0.116 ± 0.004
05855851	78.447 ± 0.189	6.411 ± 0.021	M3 V	3410	0.385 ± 0.012	0.377 ± 0.009
05941130	261.381 ± 4.693	6.178 ± 0.050	M3 V	3410	0.418 ± 0.014	0.415 ± 0.012
05966669	71.057 ± 0.363	8.367 ± 0.028	M4 V	3241	0.182 ± 0.006	0.150 ± 0.004
06029542	124.094 ± 0.960	7.314 ± 0.036	M4 V	3241	0.276 ± 0.009	0.248 ± 0.007
06060042	124.392 ± 0.785	6.448 ± 0.026	M3 V	3410	0.380 ± 0.012	0.371 ± 0.009
06099502	57.992 ± 0.161	7.144 ± 0.024	M4 V	3241	0.294 ± 0.009	0.270 ± 0.007
06110166	149.098 ± 1.591	6.428 ± 0.034	M4 V	3241	0.383 ± 0.012	0.374 ± 0.010
06181143	92.310 ± 0.508	6.470 ± 0.025	M4 V	3241	0.377 ± 0.011	0.368 ± 0.009
06201164	41.383 ± 0.113	8.606 ± 0.019	M5 V	3073	0.166 ± 0.005	0.135 ± 0.003
06209585	74.533 ± 0.310	8.121 ± 0.027	M4 V	3241	0.201 ± 0.006	0.168 ± 0.004
06365513	82.925 ± 0.595	5.800 ± 0.024	M4 V	3241	0.475 ± 0.014	0.477 ± 0.011
06423922	85.563 ± 0.277	6.720 ± 0.020	M4 V	3241	0.345 ± 0.010	0.329 ± 0.008
06431170	266.684 ± 26.668	8.573 ± 0.332	M4 V	3241	0.169 ± 0.021	0.137 ± 0.020
06460812	147.694 ± 1.953	6.097 ± 0.035	M3 V	3410	0.430 ± 0.013	0.428 ± 0.011

Table 4 continued

Table 4 (*continued*)

KIC ID	Distance	M_{K_S}	Spec. Type	T_{eff}^a	R_*	M_*
	(pc)	(mag)		(K)	(R_{\odot})	(M_{\odot})
06507276	133.950 ± 0.723	6.804 ± 0.027	M3 V	0	0.334 ± 0.010	0.317 ± 0.008
06510539	188.951 ± 2.064	6.791 ± 0.035	M3 V	3410	0.336 ± 0.011	0.319 ± 0.009
06580019	121.275 ± 1.934	8.594 ± 0.063	M5 V	3073	0.167 ± 0.006	0.136 ± 0.005
06751111	94.861 ± 1.771	7.503 ± 0.046	M5 V	3073	0.256 ± 0.009	0.226 ± 0.007
06784660	72.266 ± 0.235	7.645 ± 0.018	M4 V	3241	0.242 ± 0.007	0.211 ± 0.005
06925256	132.365 ± 0.997	6.538 ± 0.026	M3 V	3410	0.368 ± 0.011	0.357 ± 0.009
07025613	128.887 ± 3.234	8.661 ± 0.079	M5 V	3073	0.163 ± 0.007	0.132 ± 0.005
07033670	18.131 ± 0.017	8.319 ± 0.017	M6 V	2904	0.186 ± 0.006	0.153 ± 0.004
07094638	106.769 ± 0.708	7.346 ± 0.029	M4 V	3241	0.272 ± 0.008	0.244 ± 0.006
07094777	123.682 ± 0.755	6.137 ± 0.023	M4 V	3241	0.424 ± 0.013	0.422 ± 0.010
07100573	207.135 ± 2.117	6.014 ± 0.034	M4 V	3241	0.442 ± 0.014	0.442 ± 0.011
07265390	103.052 ± 0.634	7.440 ± 0.027	M4 V	3241	0.262 ± 0.008	0.233 ± 0.006
07298281	79.796 ± 0.328	6.875 ± 0.017	M4 V	3241	0.326 ± 0.010	0.306 ± 0.007
07341517	129.666 ± 1.412	7.820 ± 0.048	M4 V	3241	0.226 ± 0.008	0.194 ± 0.006
07350394	116.340 ± 0.643	6.926 ± 0.022	M3 V	3410	0.319 ± 0.010	0.299 ± 0.007
07435842	37.067 ± 0.110	9.241 ± 0.020	M6 V	2904	0.133 ± 0.004	0.106 ± 0.003
07663056	123.455 ± 1.233	7.755 ± 0.043	M5 V	3073	0.232 ± 0.008	0.200 ± 0.006
07668390	155.626 ± 1.664	7.179 ± 0.035	M4 V	3241	0.290 ± 0.009	0.265 ± 0.007
07676799	142.090 ± 1.472	6.786 ± 0.030	M4 V	3241	0.337 ± 0.010	0.319 ± 0.008
07678417	122.180 ± 1.135	6.068 ± 0.024	M4 V	3241	0.434 ± 0.013	0.433 ± 0.010
07691437	26.760 ± 0.056	9.649 ± 0.020	M7 V	2736	0.119 ± 0.003	0.094 ± 0.002
07731089	166.665 ± 1.493	7.060 ± 0.035	M3 V	3410	0.304 ± 0.010	0.281 ± 0.008
07731963	247.742 ± 4.437	6.357 ± 0.056	M3 V	3410	0.393 ± 0.014	0.386 ± 0.012
07739468	201.036 ± 2.362	6.665 ± 0.036	M3 V	3410	0.352 ± 0.011	0.337 ± 0.009
07757418	169.535 ± 1.359	6.560 ± 0.036	M4 V	3241	0.365 ± 0.012	0.354 ± 0.010
07799941	69.023 ± 0.453	8.664 ± 0.028	M7 V	2736	0.163 ± 0.005	0.132 ± 0.003
07820535	49.419 ± 0.128	7.307 ± 0.017	M4 V	3241	0.276 ± 0.008	0.249 ± 0.006
07830804	95.992 ± 0.697	8.102 ± 0.035	M4 V	3241	0.202 ± 0.006	0.169 ± 0.005
07941437	166.655 ± 2.091	5.236 ± 0.031	M4 V	3241	0.569 ± 0.017	0.567 ± 0.014
07957625	120.601 ± 1.252	7.709 ± 0.036	M4 V	3241	0.236 ± 0.008	0.204 ± 0.006
07960044	135.460 ± 1.997	5.981 ± 0.037	M5 V	3073	0.447 ± 0.014	0.447 ± 0.012
08154114	29.472 ± 0.031	7.619 ± 0.011	M5 V	3073	0.245 ± 0.007	0.214 ± 0.005
08221528	148.876 ± 1.703	7.754 ± 0.050	M3 V	3410	0.232 ± 0.008	0.200 ± 0.007
08222581	154.952 ± 1.444	6.887 ± 0.031	M3 V	3410	0.324 ± 0.010	0.305 ± 0.008
08247428	153.994 ± 3.140	8.380 ± 0.082	M4 V	3241	0.181 ± 0.008	0.149 ± 0.006
08393988	97.377 ± 0.440	7.329 ± 0.029	M3 V	3410	0.274 ± 0.008	0.246 ± 0.006
08408875	49.072 ± 0.108	6.258 ± 0.012	M4 V	3241	0.407 ± 0.012	0.402 ± 0.009
08409924	299.875 ± 6.498	5.898 ± 0.055	M4 V	3241	0.459 ± 0.016	0.461 ± 0.014
08414250	185.079 ± 2.646	6.258 ± 0.040	M4 V	3241	0.407 ± 0.013	0.402 ± 0.011
08489264	108.453 ± 0.517	7.121 ± 0.018	M2 V	3578	0.297 ± 0.009	0.273 ± 0.006

Table 4 continued

Table 4 (*continued*)

KIC ID	Distance	M_{K_S}	Spec. Type	T_{eff}^a	R_*	M_*
	(pc)	(mag)		(K)	(R_{\odot})	(M_{\odot})
08526622	157.750 ± 2.551	7.179 ± 0.063	M4 V	3241	0.290 ± 0.011	0.265 ± 0.010
08557567	135.302 ± 1.259	7.180 ± 0.030	M4 V	3241	0.290 ± 0.009	0.265 ± 0.007
08573327	134.691 ± 1.544	7.412 ± 0.036	M4 V	3241	0.265 ± 0.009	0.237 ± 0.007
08604803	160.616 ± 1.523	6.733 ± 0.030	M3 V	3410	0.343 ± 0.011	0.327 ± 0.008
08631743	156.018 ± 2.201	7.973 ± 0.062	M4 V	3241	0.213 ± 0.008	0.180 ± 0.007
08673562	61.976 ± 0.229	8.266 ± 0.024	M6 V	2904	0.190 ± 0.006	0.157 ± 0.004
08735884	96.715 ± 0.356	7.167 ± 0.024	M3 V	3410	0.292 ± 0.009	0.267 ± 0.007
08738977	133.189 ± 1.951	8.346 ± 0.073	M5 V	3073	0.184 ± 0.007	0.151 ± 0.006
08825565	112.247 ± 0.735	6.959 ± 0.024	M4 V	3241	0.315 ± 0.010	0.295 ± 0.007
08846163	63.727 ± 0.388	5.555 ± 0.023	M4 V	3241	0.515 ± 0.015	0.517 ± 0.013
08878564	162.228 ± 1.783	7.327 ± 0.042	M3 V	3410	0.274 ± 0.009	0.247 ± 0.007
08881388	103.788 ± 0.687	7.296 ± 0.024	M5 V	3073	0.278 ± 0.008	0.250 ± 0.006
08888573	64.164 ± 0.117	6.434 ± 0.020	M3 V	3410	0.382 ± 0.011	0.373 ± 0.009
08935655	55.855 ± 0.103	6.231 ± 0.015	M4 V	3241	0.410 ± 0.012	0.406 ± 0.009
08935942	125.198 ± 1.113	6.975 ± 0.032	M5 V	3073	0.314 ± 0.010	0.292 ± 0.008
09006264	62.430 ± 0.179	6.662 ± 0.018	M5 V	3073	0.352 ± 0.010	0.338 ± 0.008
09028977	140.544 ± 5.408	5.749 ± 0.085	M3 V	3410	0.483 ± 0.019	0.485 ± 0.018
09033543	20.468 ± 0.026	8.824 ± 0.012	M6 V	2904	0.154 ± 0.004	0.123 ± 0.003
09048032	131.835 ± 1.344	6.756 ± 0.030	M4 V	3241	0.340 ± 0.011	0.324 ± 0.008
09090909	M3 V	3410	0.341 ± 0.064	0.321 ± 0.093
09111293	86.723 ± 0.351	7.479 ± 0.023	M3 V	3410	0.259 ± 0.008	0.229 ± 0.006
09153593	112.179 ± 0.678	6.790 ± 0.020	M4 V	3241	0.336 ± 0.010	0.319 ± 0.008
09153754	45.638 ± 0.186	6.799 ± 0.017	M5 V	3073	0.335 ± 0.010	0.317 ± 0.007
09201463	M5 V	3073	0.190 ± 0.040	0.153 ± 0.052
09210374	119.012 ± 0.546	6.359 ± 0.016	M3 V	3410	0.392 ± 0.012	0.385 ± 0.009
09268481	M4 V	3241	0.258 ± 0.053	0.226 ± 0.075
09282187	51.318 ± 0.253	9.200 ± 0.031	M7 V	2736	0.135 ± 0.004	0.107 ± 0.003
09326073	94.173 ± 4.937	7.818 ± 0.117	M4 V	3241	0.226 ± 0.012	0.194 ± 0.012
09391230	224.339 ± 2.964	6.478 ± 0.046	M4 V	3241	0.376 ± 0.013	0.366 ± 0.011
09396972	73.708 ± 0.309	7.960 ± 0.021	M4 V	3241	0.214 ± 0.006	0.181 ± 0.004
09401964	147.359 ± 1.008	6.556 ± 0.025	M4 V	3241	0.366 ± 0.011	0.354 ± 0.009
09471335	96.306 ± 0.391	6.662 ± 0.021	M4 V	3241	0.352 ± 0.011	0.338 ± 0.008
09475080	127.827 ± 1.532	7.709 ± 0.041	M5 V	3073	0.236 ± 0.008	0.204 ± 0.006
09476089	293.072 ± 13.572	7.729 ± 0.173	M4 V	3241	0.234 ± 0.017	0.202 ± 0.018
09516961	159.734 ± 1.168	6.194 ± 0.024	M4 V	3241	0.416 ± 0.013	0.412 ± 0.010
09517514	136.730 ± 2.445	8.302 ± 0.060	M5 V	3073	0.187 ± 0.007	0.154 ± 0.005
09530715	66.720 ± 0.540	7.928 ± 0.028	M5 V	3073	0.217 ± 0.007	0.184 ± 0.005
09533040	247.921 ± 9.317	7.445 ± 0.117	M4 V	3241	0.262 ± 0.014	0.233 ± 0.014
09579384	M3 V	3410	0.341 ± 0.064	0.321 ± 0.093
09581479	210.875 ± 6.580	8.099 ± 0.116	M4 V	3241	0.203 ± 0.011	0.169 ± 0.010

Table 4 continued

Table 4 (*continued*)

KIC ID	Distance	M_{K_S}	Spec. Type	T_{eff}^a	R_*	M_*
	(pc)	(mag)		(K)	(R_{\odot})	(M_{\odot})
09593909	226.925 ± 4.217	6.932 ± 0.061	M4 V	3241	0.319 ± 0.012	0.298 ± 0.011
09631940	313.922 ± 6.353	5.747 ± 0.053	M4 V	3241	0.483 ± 0.016	0.485 ± 0.014
09636945	420.348 ± 20.946	4.981 ± 0.115	M2 V	3578	0.615 ± 0.027	0.604 ± 0.022
09645092	85.618 ± 0.379	7.770 ± 0.021	M4 V	3241	0.231 ± 0.007	0.198 ± 0.005
09653548	158.912 ± 1.754	7.349 ± 0.044	M4 V	3241	0.272 ± 0.009	0.244 ± 0.008
09654304	288.559 ± 7.006	6.307 ± 0.070	M4 V	3241	0.400 ± 0.015	0.394 ± 0.014
09655322	720.455 ± 69.437	5.674 ± 0.251	M4 V	3241	0.495 ± 0.043	0.498 ± 0.042
09655551	361.087 ± 31.610	6.927 ± 0.220	M4 V	3241	0.320 ± 0.027	0.300 ± 0.032
09655667	290.477 ± 15.055	7.362 ± 0.155	M4 V	3241	0.271 ± 0.018	0.243 ± 0.019
09659082	68.703 ± 0.299	6.731 ± 0.020	M4 V	3241	0.343 ± 0.010	0.328 ± 0.008
09710717	256.815 ± 4.845	6.201 ± 0.058	M3 V	3410	0.415 ± 0.015	0.411 ± 0.013
09711491	70.303 ± 0.291	7.921 ± 0.023	M4 V	3241	0.217 ± 0.007	0.184 ± 0.005
09754582	151.578 ± 1.532	7.132 ± 0.040	M4 V	3241	0.296 ± 0.010	0.271 ± 0.008
09784820	145.863 ± 1.518	6.948 ± 0.033	M4 V	3241	0.317 ± 0.010	0.296 ± 0.008
09817857	80.399 ± 0.440	7.825 ± 0.025	M5 V	3073	0.226 ± 0.007	0.193 ± 0.005
09826844	179.877 ± 1.265	5.744 ± 0.027	M2 V	3578	0.484 ± 0.015	0.486 ± 0.012
09837302	382.284 ± 16.206	6.231 ± 0.117	M3 V	3410	0.410 ± 0.021	0.405 ± 0.021
09912373	309.361 ± 7.530	5.641 ± 0.060	M4 V	3241	0.501 ± 0.017	0.503 ± 0.015
09933524	175.961 ± 2.546	7.081 ± 0.051	M5 V	3073	0.301 ± 0.010	0.278 ± 0.009
09942231	205.718 ± 3.203	6.260 ± 0.042	M5 V	3073	0.406 ± 0.013	0.401 ± 0.011
10004407	112.784 ± 0.452	6.785 ± 0.019	M3 V	3410	0.337 ± 0.010	0.320 ± 0.008
10053146	53.212 ± 0.844	9.637 ± 0.042	M8 V	2568	0.120 ± 0.004	0.094 ± 0.003
10057002	M7 V	2736	0.126 ± 0.018	0.091 ± 0.018
10057939	98.997 ± 0.415	7.139 ± 0.024	M4 V	3241	0.295 ± 0.009	0.270 ± 0.007
10118794	95.844 ± 1.437	8.701 ± 0.056	M7 V	2736	0.161 ± 0.006	0.130 ± 0.004
10158029	168.795 ± 9.600	6.010 ± 0.126	M4 V	3241	0.443 ± 0.023	0.442 ± 0.023
10186824	M3 V	3410	0.341 ± 0.064	0.321 ± 0.093
10267155	187.400 ± 2.037	6.571 ± 0.035	M4 V	3241	0.364 ± 0.012	0.352 ± 0.010
10273058	99.972 ± 0.452	6.989 ± 0.020	M4 V	3241	0.312 ± 0.009	0.290 ± 0.007
10274090	137.271 ± 0.831	6.116 ± 0.023	M4 V	3241	0.427 ± 0.013	0.425 ± 0.010
10320084	111.810 ± 0.683	7.701 ± 0.035	M3 V	3410	0.237 ± 0.008	0.205 ± 0.006
10322878	68.535 ± 0.294	7.530 ± 0.020	M5 V	3073	0.253 ± 0.008	0.223 ± 0.005
10339105	43.328 ± 0.648	6.443 ± 0.036	M4 V	3241	0.381 ± 0.012	0.372 ± 0.010
10345684	151.964 ± 2.231	7.610 ± 0.053	M5 V	3073	0.246 ± 0.009	0.215 ± 0.007
10453314	36.548 ± 0.049	6.648 ± 0.019	M4 V	3241	0.354 ± 0.011	0.340 ± 0.008
10456779	292.784 ± 5.106	5.960 ± 0.054	M3 V	3410	0.450 ± 0.015	0.450 ± 0.013
10522057	214.971 ± 2.480	5.491 ± 0.035	M3 V	3410	0.525 ± 0.016	0.527 ± 0.013
10557342	111.411 ± 0.502	6.599 ± 0.026	M3 V	3410	0.360 ± 0.011	0.348 ± 0.009
10598142	106.170 ± 0.340	6.394 ± 0.017	M3 V	3410	0.388 ± 0.011	0.380 ± 0.009
10649277	83.468 ± 2.980	7.424 ± 0.081	M5 V	3073	0.264 ± 0.011	0.235 ± 0.011

Table 4 continued

Table 4 (*continued*)

KIC ID	Distance	M_{K_S}	Spec. Type	T_{eff}^a	R_*	M_*
	(pc)	(mag)		(K)	(R_{\odot})	(M_{\odot})
10651319	281.639 ± 4.938	5.914 ± 0.052	M3 V	3410	0.457 ± 0.015	0.458 ± 0.013
10659335	202.974 ± 2.140	6.369 ± 0.032	M3 V	3410	0.391 ± 0.012	0.384 ± 0.010
10784750	199.051 ± 1.689	5.809 ± 0.031	M3 V	3410	0.474 ± 0.015	0.475 ± 0.012
10819154	134.956 ± 1.093	7.208 ± 0.039	M4 V	3241	0.287 ± 0.009	0.261 ± 0.008
10877432	48.968 ± 0.070	7.212 ± 0.017	M4 V	3241	0.287 ± 0.008	0.261 ± 0.006
10905192	113.531 ± 1.031	7.487 ± 0.035	M5 V	3073	0.258 ± 0.008	0.228 ± 0.006
10907400	99.376 ± 0.393	6.348 ± 0.019	M3 V	3410	0.394 ± 0.012	0.387 ± 0.009
10911018	30.428 ± 0.037	7.465 ± 0.022	M6 V	2904	0.260 ± 0.008	0.230 ± 0.006
10924100	314.613 ± 19.120	5.607 ± 0.136	M4 V	3241	0.506 ± 0.027	0.508 ± 0.025
10932417	97.838 ± 0.760	6.388 ± 0.024	M4 V	3241	0.388 ± 0.012	0.381 ± 0.009
10963537	M4 V	3241	0.258 ± 0.053	0.226 ± 0.075
10991155	244.474 ± 3.268	4.562 ± 0.037	M4 V	3241	0.258 ± 0.053	0.226 ± 0.075
11025770	109.753 ± 0.579	5.708 ± 0.024	M3 V	3410	0.490 ± 0.015	0.492 ± 0.012
11027877	132.839 ± 0.758	6.661 ± 0.030	M3 V	3410	0.352 ± 0.011	0.338 ± 0.009
11126343	M4 V	3241	0.258 ± 0.053	0.226 ± 0.075
11175934	144.056 ± 1.600	7.621 ± 0.051	M5 V	3073	0.245 ± 0.009	0.213 ± 0.007
11196417	231.232 ± 3.094	4.530 ± 0.034	M5 V	3073	0.190 ± 0.040	0.153 ± 0.052
11237082	144.070 ± 1.402	7.142 ± 0.036	M4 V	3241	0.294 ± 0.009	0.270 ± 0.008
11251839	132.847 ± 0.633	5.979 ± 0.020	M4 V	3241	0.447 ± 0.013	0.447 ± 0.011
11293949	51.681 ± 0.111	6.924 ± 0.019	M5 V	3073	0.320 ± 0.010	0.300 ± 0.007
11295657	187.969 ± 2.439	7.321 ± 0.052	M3 V	3410	0.275 ± 0.010	0.247 ± 0.008
11389346	317.078 ± 7.038	5.632 ± 0.060	M4 V	3241	0.502 ± 0.017	0.504 ± 0.015
11400756	60.038 ± 0.196	7.554 ± 0.027	M3 V	3410	0.251 ± 0.008	0.221 ± 0.006
11442458	85.439 ± 0.313	7.267 ± 0.026	M4 V	3241	0.281 ± 0.009	0.254 ± 0.006
11456603	157.833 ± 1.477	6.111 ± 0.030	M4 V	3241	0.428 ± 0.013	0.426 ± 0.011
11503101	134.850 ± 2.091	6.555 ± 0.042	M4 V	3241	0.366 ± 0.012	0.354 ± 0.010
11548779	192.349 ± 1.989	6.173 ± 0.034	M3 V	3410	0.419 ± 0.013	0.416 ± 0.011
11550104	97.104 ± 1.345	9.071 ± 0.070	M7 V	2736	0.141 ± 0.005	0.112 ± 0.004
11558721	173.528 ± 1.034	5.576 ± 0.022	M3 V	3410	0.511 ± 0.015	0.513 ± 0.012
11597669	58.284 ± 0.185	8.066 ± 0.019	M4 V	3241	0.205 ± 0.006	0.172 ± 0.004
11612157	183.820 ± 4.104	5.911 ± 0.052	M3 V	3410	0.458 ± 0.016	0.459 ± 0.013
11612159	190.314 ± 2.405	6.595 ± 0.041	M3 V	3410	0.361 ± 0.012	0.348 ± 0.010
11652732	107.877 ± 0.487	7.002 ± 0.025	M3 V	3410	0.310 ± 0.009	0.289 ± 0.007
11654120	101.497 ± 2.453	9.082 ± 0.080	M6 V	2904	0.140 ± 0.006	0.112 ± 0.004
11709022	64.302 ± 3.803	4.634 ± 0.131	M4 V	3241	0.681 ± 0.032	0.654 ± 0.025
11855853	219.865 ± 3.208	6.544 ± 0.050	M3 V	3410	0.367 ± 0.013	0.356 ± 0.011
11862609	159.117 ± 2.020	7.361 ± 0.050	M4 V	3241	0.271 ± 0.009	0.243 ± 0.008
12071873	217.540 ± 2.293	5.264 ± 0.030	M3 V	3410	0.564 ± 0.017	0.562 ± 0.014
12101934	141.893 ± 1.056	7.032 ± 0.033	M4 V	3241	0.307 ± 0.010	0.285 ± 0.008
12102994	301.489 ± 5.265	5.756 ± 0.052	M3 V	3410	0.482 ± 0.016	0.484 ± 0.014

Table 4 continued

Table 4 (*continued*)

KIC ID	Distance	M_{K_S}	Spec. Type	T_{eff}^a	R_*	M_*
	(pc)	(mag)		(K)	(R_{\odot})	(M_{\odot})
12117672	121.713 ± 1.296	8.153 ± 0.052	M5 V	3073	0.198 ± 0.007	0.165 ± 0.005
12156321	162.902 ± 1.262	6.223 ± 0.029	M4 V	3241	0.412 ± 0.013	0.407 ± 0.010
12168731	249.094 ± 6.406	7.181 ± 0.093	M4 V	3241	0.290 ± 0.013	0.265 ± 0.013
12305237	80.201 ± 0.205	6.560 ± 0.020	M3 V	3410	0.365 ± 0.011	0.354 ± 0.008
12508767	75.955 ± 0.209	6.763 ± 0.026	M3 V	3410	0.339 ± 0.010	0.323 ± 0.008
12645891	199.484 ± 3.660	7.136 ± 0.060	M4 V	3241	0.295 ± 0.011	0.271 ± 0.010
12735831	68.308 ± 0.228	7.990 ± 0.024	M4 V	3241	0.212 ± 0.006	0.178 ± 0.004
12784248	79.894 ± 0.657	8.889 ± 0.032	M6 V	2904	0.150 ± 0.005	0.120 ± 0.003
12884812	126.624 ± 1.008	7.013 ± 0.030	M2 V	3578	0.309 ± 0.010	0.287 ± 0.008

^aWe adopt a ± 88 K uncertainty for all temperatures from our spectral type vs. T_{eff} fit (Section 3.3).